
Masters Theses

Student Theses and Dissertations

1966

The Faraday rotation and dispersive doppler effects in the ionosphere at oblique incidence

Charles Roland Baugher II

Follow this and additional works at: https://scholarsmine.mst.edu/masters_theses



Part of the [Physics Commons](#)

Department:

Recommended Citation

Baugher, Charles Roland II, "The Faraday rotation and dispersive doppler effects in the ionosphere at oblique incidence" (1966). *Masters Theses*. 5755.

https://scholarsmine.mst.edu/masters_theses/5755

This thesis is brought to you by Scholars' Mine, a service of the Missouri S&T Library and Learning Resources. This work is protected by U. S. Copyright Law. Unauthorized use including reproduction for redistribution requires the permission of the copyright holder. For more information, please contact scholarsmine@mst.edu.

THE FARADAY ROTATION AND DISPERSIVE DOPPLER EFFECTS
IN THE IONOSPHERE AT OBLIQUE INCIDENCE

by

Charles Roland Baugher, II

A
THESIS

submitted to the faculty of
THE UNIVERSITY OF MISSOURI AT ROLLA
in partial fulfillment of the requirements for the

Degree of
MASTER OF SCIENCE, PHYSICS MAJOR

Rolla, Missouri

1966

Approved by

Harold D. Fuller (advisor)
Charles E. Antle

Charles E. MacFarland
Charles A. Johnson

ABSTRACT

Integral equations for the isotropic and anisotropic ray path of a radio wave propagating through the ionosphere are developed. These equations assume a spherically stratified ionosphere and are equivalent to a detailed ray-tracing process. A method is devised to utilize these equations in the evaluation of combined Faraday rotation and dispersive Doppler data from earth satellites for subionospheric electron content. The method, which corrects for horizontal ionospheric gradients, is applied to data from the Explorer 22 satellite and some preliminary results are discussed.

ACKNOWLEDGMENTS

The author is indebted to many people for help and encouragement in the preparation of this work: in particular, to Dr. Harold Fuller at the University of Missouri and Dr. Eugene Mechtly at Marshall Space Flight Center. The assistance of Mr. Fred Rodrigue in the computer programming and Mr. William Edens in the data recording is gratefully acknowledged.

TABLE OF CONTENTS

	Page
ACKNOWLEDGMENTS	iii
ILLUSTRATIONS AND TABLES	v
GLOSSARY	vi
I. INTRODUCTION	1
II. DATA RECORDING AND REDUCTION	5
III. MAGNETO-IONIC THEORY	18
A. The Appleton-Hartree Equation	20
B. Approximations to the Appleton-Hartree Equation	27
C. Propagation in an Anisotropic Medium	29
D. The Faraday Rotation Effect	35
E. The Dispersive Doppler Effect	40
IV. THE RAY PATH LENGTH FOR OBLIQUE INCIDENCE	43
A. The Isotropic Ray Path	44
B. The Anisotropic Ray Path	50
V. THE FARADAY ROTATION AND DISPERSIVE DOPPLER EQUATIONS	58
VI. METHOD OF ANALYSIS	63
VII. RESULTS OF ANALYSIS	70
VIII. CONCLUSIONS	82
IX. BIBLIOGRAPHY	84
X. VITA	86

ILLUSTRATIONS AND TABLES

	Page
1. Green Mountain Radio Propagation Test Site, Huntsville, Alabama	6
2. Ionospheric Data from Explorer 22 (Huntsville, Alabama, 16:20 CST, 10/29/64)	8
3. Ionospheric Data from Explorer 22 (Huntsville, Alabama, 04:24 CST, 10/31/64)	9
4. 20 and 40 MHz Dipole Antenna	10
5. Ionosphere Beacon Data Receiving & Recording Equipment	11
6. Ionosphere Beacon Receiver	12
7. Tracking Antenna (Green Mountain)	14
8. 360 MHz Yagi Antenna System	16
9. Wave Velocity Surfaces ($\frac{1}{\mu}$)	30
10. Geometry for Calculating α	33
11. Geometry for the Ray Path	45
12. Bouguer's Rule	47
13. Ordinary and Extraordinary Ray Directions	53
14. Relation Between dh and ds_e	55
15. Doppler Shift Offset vs. N_{\max}	62
16. Subionosphere Point	69
17. Electron Content vs. Satellite Elevation	74
18. Ionosphere Variation Ratio vs. Satellite Elevation	76
19. Faraday Rotations vs. Satellite Elevation	80
 Tables	
1. Recorded Data and the Position of the Satellite Relative to the Green Mountain Station	72
2. Results of the Analysis	73

GLOSSARY

LIST OF SYMBOLS

α	Angle between the wave normal and ray
α'	Angle between the wave normal and the projection of the ray onto the plane of incidence
α''	Angle between the ray and the plane of incidence
\vec{B}	Geomagnetic field flux density
θ	Faraday rotation angle
C	Doppler shift offset
c	Speed of light
\vec{D}	Displacement
E	Ionosphere variation ratio
\vec{E}	Electric field strength
e	Electronic charge
ϵ_0	Permittivity of free space
F	Dispersive Doppler frequency
f	Frequency
G	Ratio between Faraday rotations and Doppler shift offset
H	Scale height

LIST OF SYMBOLS

continued -

\vec{H}	Magnetic field intensity
h_m	Height of maximum ionization
h_s	Height of the satellite
η	Number of dispersive Doppler cycles observed during Δt
θ	Angle between the wave normal and the geomagnetic field
i	$\sqrt{-1}$
λ	Wavelength
m	Electronic mass
μ	Index of refraction
μ_e	Extraordinary index of refraction
μ_f	Isotropic refractive index at frequency f
μ_{mf}	Isotropic refractive index at frequency mf
μ_o	Ordinary index of refraction
μ_o	Permeability of free space
N	Electron density
N_{max}	Maximum electron density
N_T	Columnar electron content

LIST OF SYMBOLS

continued -

n	Refractive index
ν	Electron collisions frequency
\bar{p}	Electric moment per unit volume
P_e	Extraordinary phase path
P_f	Isotropic phase path at frequency f
P_{mf}	Isotropic phase path at frequency mf
P_o	Ordinary phase path
R	Radius of the earth
R_s	Range from the station to the satellite
S	Ray path
S_e	Extraordinary ray path
S_f	Isotropic ray path at frequency f
S_{mf}	Isotropic ray path at frequency mf
S_o	Ordinary ray path
t	Time
τ	Time interval
v	Phase velocity

LIST OF SYMBOLS

continued -

v_r	Ray velocity
θ	Angle between the ray and the geomagnetic field
\hat{w}_o	Unit vector in the direction of the ordinary wave normal
\hat{w}_e	Unit vector in the direction of the extraordinary wave normal
X	$\frac{N e^2}{\epsilon_0 m \omega^2}$
χ	Angle of incidence at geocentric differential stratifications
\vec{Y}	$\frac{e}{m \omega} \vec{B}$
Y_L	$ \vec{Y} \cos \theta$
Y_T	$ \vec{Y} \sin \theta$
ψ	Angle between the satellite and the station measured at the center of the earth
Ω	Number of complete Faraday rotation
ω	Angular frequency

UNITS

The International System of Units as defined by the Eleventh General Conference on Weights and Measures at Paris in 1960 is used throughout this paper.

ELEMENTAL UNITS

Quantity	Unit	Symbol
Length	Meter	m
Mass	Kilogram	kg
Time	Second	s
Electric Current	Ampere	A

DERIVED UNITS

Volume	Cubic Meter	m ³
Frequency	Hertz	Hz
Angular Velocity	Radian per second	rad/s
Velocity	Meter per second	m/s
Electric Field Strength	Volt per meter	V/m
Magnetic Flux		Wb

In this system, multiples are formed according to the following table:

<u>Multiples</u>	<u>Prefixes</u>	<u>Symbols</u>
10 ⁹	giga	G
10 ⁶	mega	M
10 ³	kilo	k
10 ²	hecto	h
10	deka	da

I. INTRODUCTION

Because of its influence on world-wide radio communications, the earth's ionosphere has been the subject of extensive study for several years. In order to perform an accurate, long-term analysis of the spatial, diurnal and seasonal variations in this region of the upper atmosphere, the National Aeronautics and Space Administration (NASA) placed two Beacon Explorer Satellites into earth orbits. Each of these satellites, designated Explorer 22 and Explorer 27, after successful launches on October 10, 1964 and April 29, 1965, respectively, transmits linearly polarized signals on four harmonically related frequencies (20, 40, 41, and 360 MHz). By recording these transmissions at a ground-based receiver as the satellites pass overhead, it is possible to observe the cumulative effect of the ionosphere on propagation and deduce the total amount of ionization along the ray path. This information is interpreted as the electron content in an imaginary column extending vertically from the earth's surface to the height of the satellite.

There are two phenomena which are readily detectable from observations of the transmissions and can be related to this electron content. The more prominent is a rotation in the plane of polarization

as the wave traverses the ionosphere, an effect known as Faraday rotation. The effect is a result of the anisotropic properties of the ionosphere and the number of rotations is directly proportional to the ionospheric electron content. Unfortunately, it is impossible to directly measure the exact number of these rotations; however, it is possible to observe their time rate of change as the satellite passes overhead by recording the signal level of the transmissions at a fixed dipole antenna.

The second detectable phenomenon is a slight offset in the Doppler shift frequency of the moving satellite, primarily due to refractive changes in the phase path of the radio waves as they traverse the ionosphere. This offset, however, is so small that uncertainties in the relative velocity of the satellite make absolute measurements impossible. The difficulty is avoided by making use of the dispersive properties of the ionosphere. A second, much higher frequency is transmitted in phase with the lower frequency and, at the ground-based receiver, the two transmissions are converted to some third-frequency and compared in phase. The higher frequency will be relatively unaffected by the ionosphere, but the motion of the satellite has the same proportional effect on both transmissions. When the phase comparison is made, the geometric Doppler shift is cancelled, and it is possible to measure the offset which occurs at the lower frequency rather precisely. This

phenomenon has become known as the dispersive Doppler effect.

The Beacon satellites are able to produce a measure of the entire ionosphere over a fairly large geographical area and thus have an advantage not found in most other methods of studying the ionosphere. To make use of this advantage, however, it is necessary to evaluate data received while the satellite is at a low elevation angle with respect to the horizon. This low elevation angle means the transmissions will enter and leave the ionosphere at a large angle of incidence and there will be considerable amount of refraction along the ray path. Most authors [1] avoid the problem and confine their analysis to data received from very high elevation angles.

The efforts to solve ionospheric propagation problems more exactly [2] have involved complicated techniques in which a ray is aimed from the satellite toward its point of arrival, the path traced through the intervening ionosphere with Snell's law and the amount of "miss" used to calculate a better aiming direction. Although the method produces results which are interesting and accurate, it is much too time consuming to apply to a large amount of data.

In this thesis, the integral equations for the Faraday rotation and dispersive Doppler effect in the ionosphere are developed. These equations include the effects of ionospheric refraction and are derived

with the minimum number of approximations. Since the equations can be evaluated much more easily than a detailed ray tracing technique, they are convenient to use as the basis of a method for evaluating data from the Beacon Explorer satellites. One such method is developed here. The method, which also corrects for horizontal gradients in the ionosphere, is applied to data received from the Beacon satellites and the results are discussed.

II. DATA RECORDING AND REDUCTION

At the time this work was initiated, Marshall Space Flight Center had facilities that could receive and record both Faraday rotation and dispersive Doppler data from the Beacon Explorer satellites. These facilities, located at the MSFC Radio Propagation Test Site (Figure 1) on Green Mountain near Huntsville, Alabama, were installed several years prior to record data from a predecessor to the Beacon Explorer Satellites 22 and 27. This preceding satellite (S-45) was never successfully orbited; however, the receiving equipment was compatible with Explorers 22 and 27.

The information recorded from the satellites is the signal level of the 20-, 40-, and 41-MHz beacons at a dipole antenna, the phase difference between the received 20 MHz signal and a frequency equal to one-eighteenth of the received 360-MHz beacon and the phase difference between the received 40-MHz signal and a frequency equal to one-ninth of the received 360-MHz signal.

A continuous record of the beacon's signal level, as seen by a dipole antenna, can easily be related to the time rate of change of the angle of rotation of the plane of polarization since the antenna will receive a maximum signal when the plane of polarization is parallel to



FIGURE 1 - Green Mountain Radio Propagation Test Site, Huntsville, Ala.

it, and a minimum when perpendicular. A short sample of the recorded data is shown in Figures 2 and 3. The first record was received at mid-afternoon while the second was recorded shortly after dawn and the diurnal variation is quite evident.

All of the transmissions from the beacon satellites, with the exception of the 360 MHz beacon, are received at dipole antennas (Figure 4) which are connected to the receivers by low-loss coaxial cable. The receivers (Figure 5) exhibit a noise figure of less than three decibels and a band width of 100 Hz. The block diagram of the 20 MHz receiver in Figure 6 is typical of all four receivers and is fairly self-explanatory as to their internal operation. The only difference in the separate receivers is the scheme used to obtain the 32 MHz intermediate frequency from the received frequency and the 1.00025 MHz frequency of the voltage-controlled oscillator (VCO).

It will be noted that instead of actually measuring the signal level of the transmissions, the AGC voltage is recorded so that a logarithmic response is obtained. The approximately 1 MHz output of each VCO is multiplied by the appropriate factor within the phase comparator before being beat together with the output of another VCO.

The output of the receivers and phase comparators is recorded

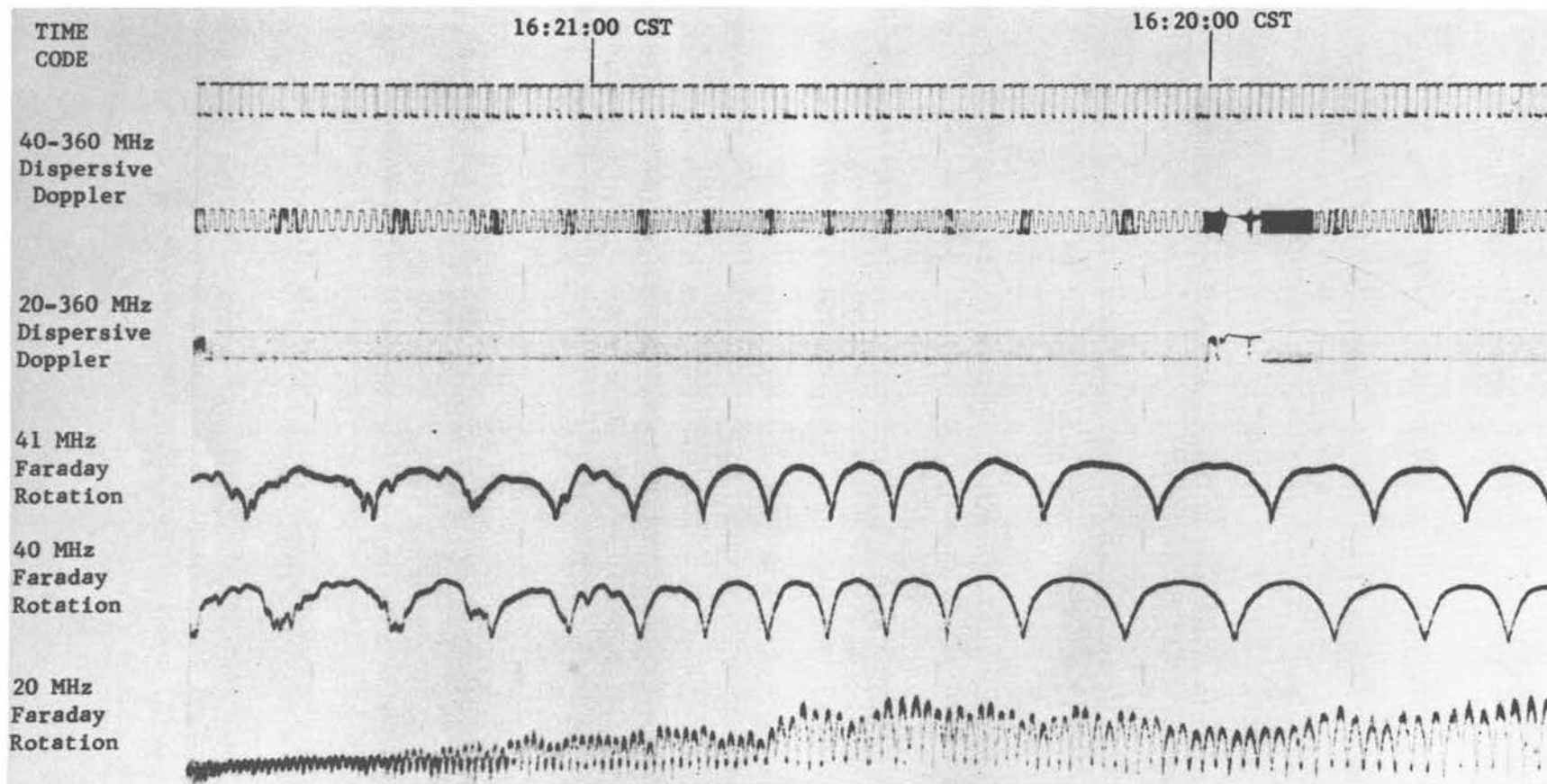


FIGURE 2 - Ionospheric Data from Explorer 22 (Huntsville, Ala., 16:20 CST, 10/29/64)

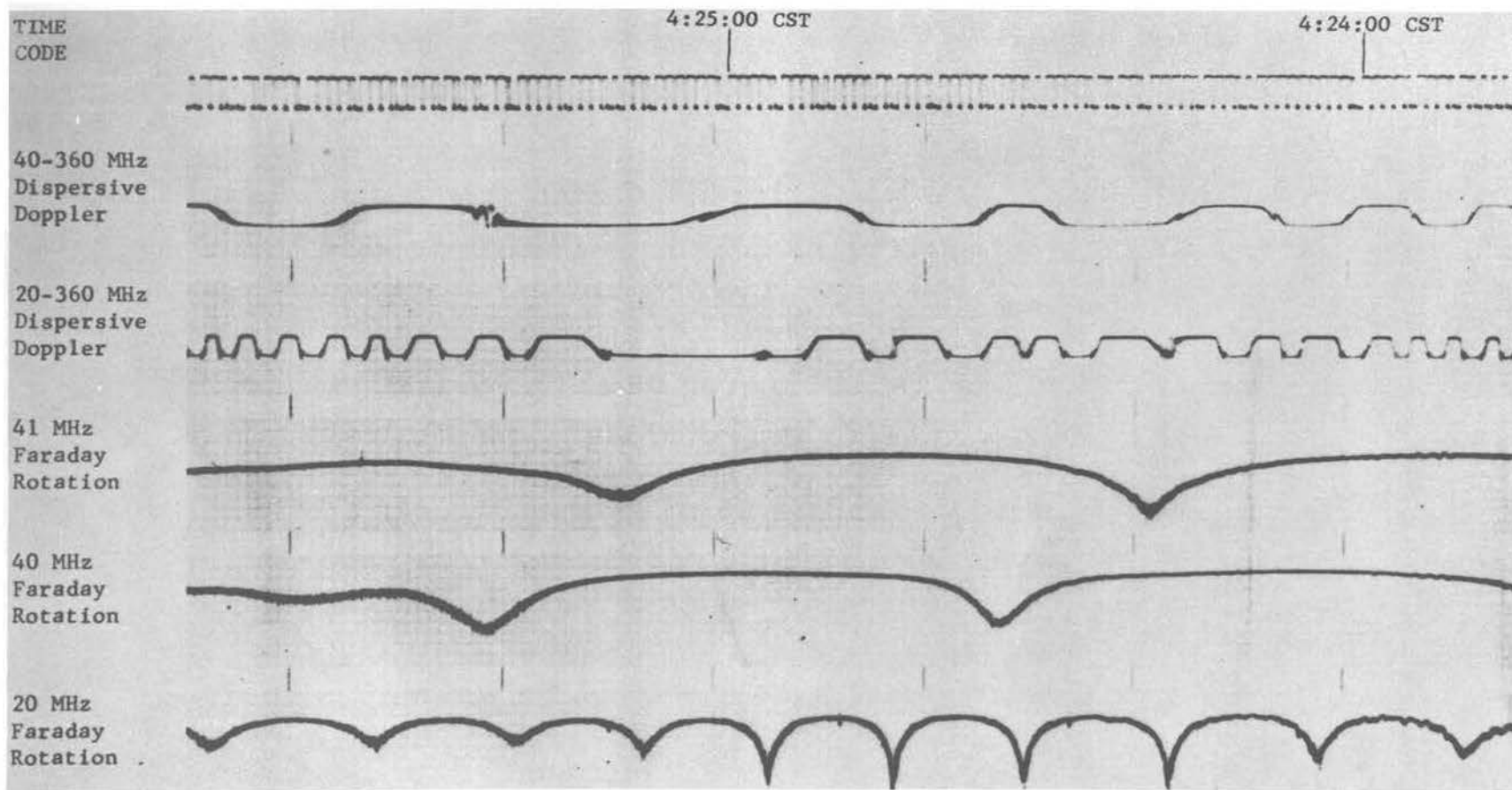


FIGURE 3 - Ionospheric Data from Explorer 22 (Huntsville, Ala., 04: 24 CST, 10/31/64)

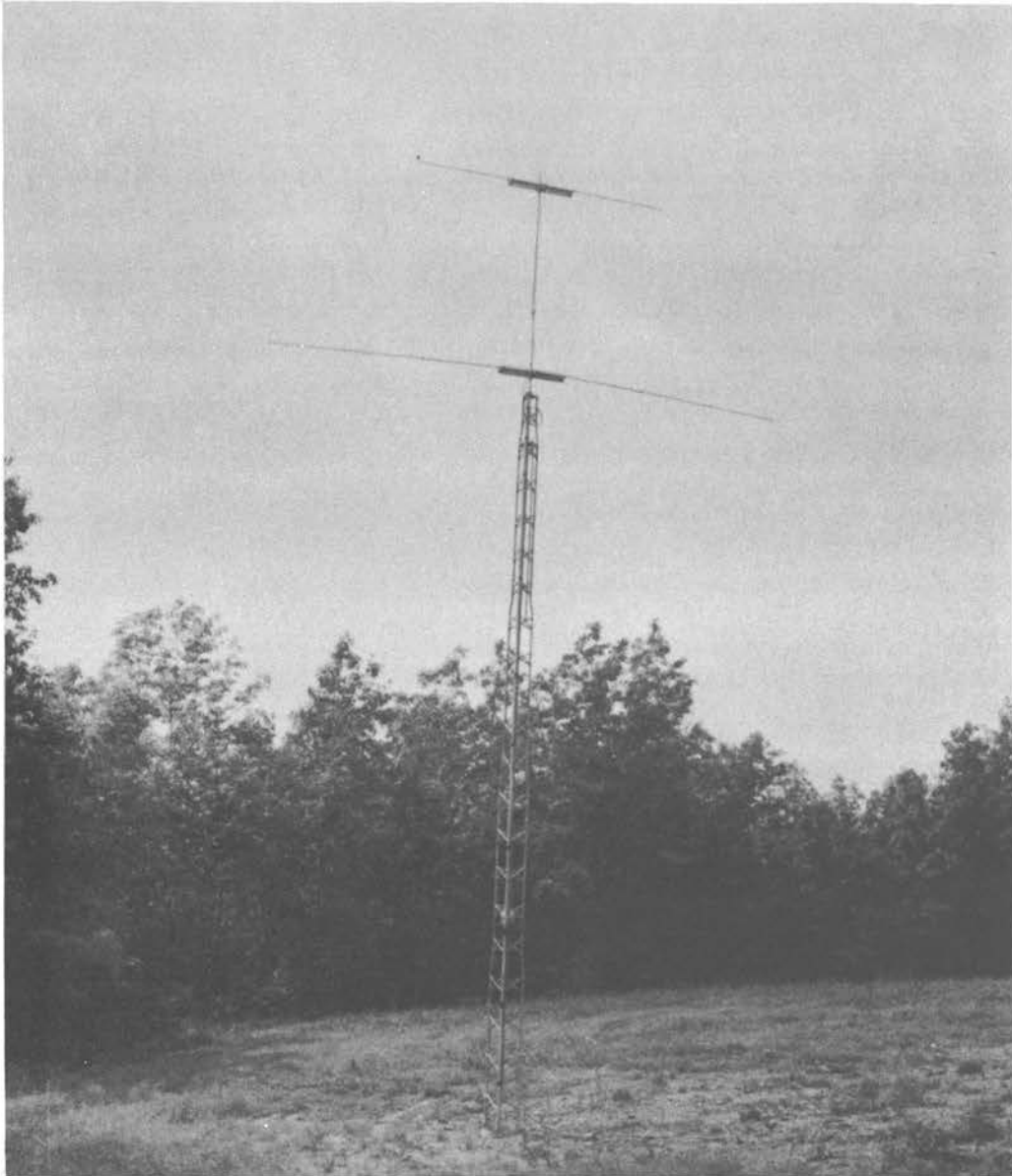


FIGURE 4 - 20 AND 40 MHz DIPOLE ANTENNA

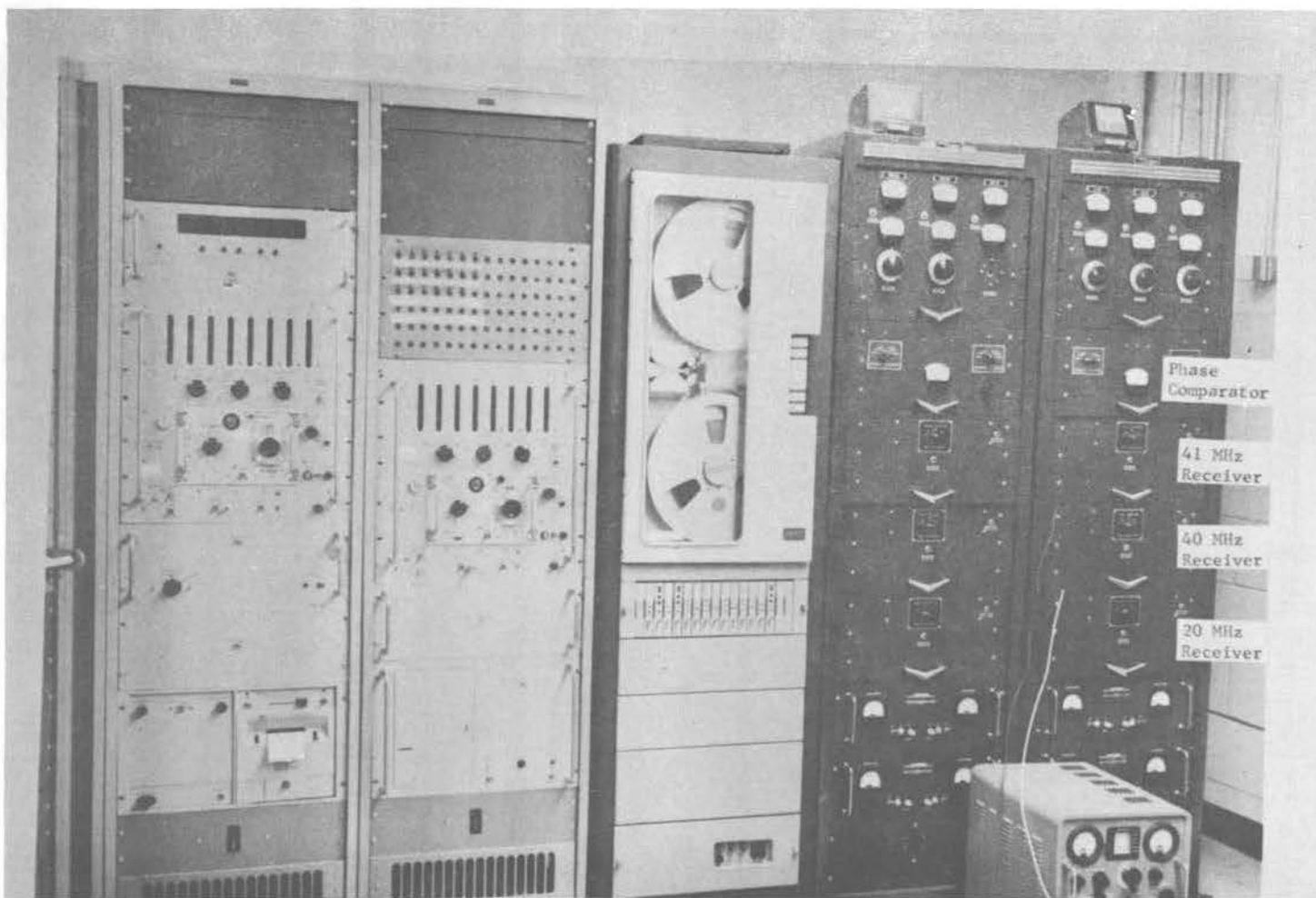


FIGURE 5 - IONOSPHERE BEACON DATA RECEIVING AND RE-
CORDING EQUIPMENT

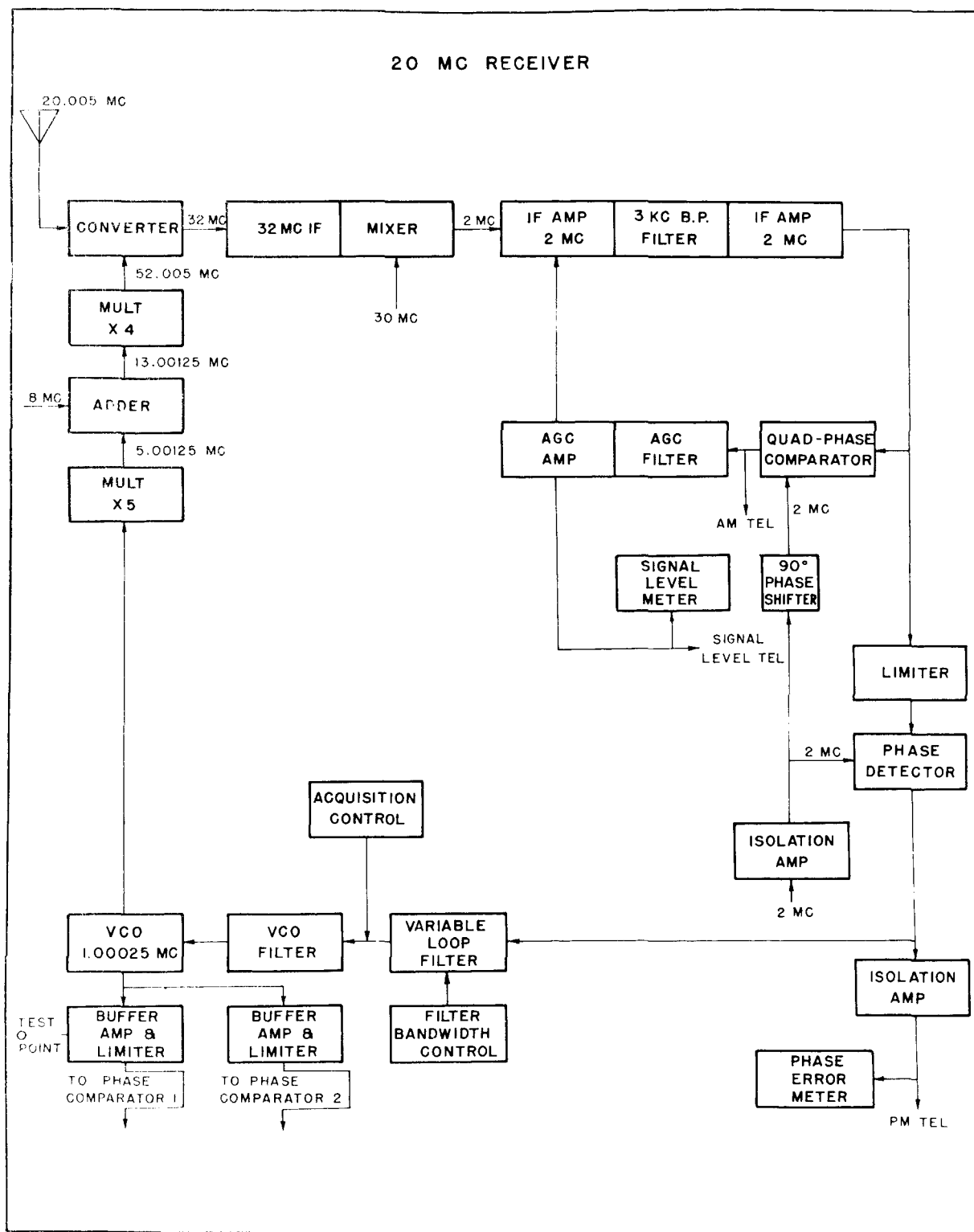


FIGURE 6 - IONOSPHERE BEACON RECEIVER

on both magnetic tape (for permanent storage) and on oscillographic strip charts (for immediate reduction). In addition to the five channels of data which are recorded during each pass of the satellite, a timing channel is also recorded. The time is recorded in a binary coded format, thus requiring seventeen bits for the exact hour, minute, and second. This information is recorded at one bit per second and after each seventeen bits, three index markers are recorded. Thus, the exact time is recorded each twenty seconds, and since the bits are exactly one second apart, it is possible to make accurate time determinations at any point on the records. This timing code is transmitted to the data recording site from the nearby MSFC on a 226.5 MHz carrier. At its origin, the timing is continually synchronized with the National Bureau of Standard's WWV radio transmissions from Washington, D. C., and is accurate to within a few milliseconds.

The major problem which occurred at the Green Mountain site after the launch of the first satellite was in the reception of the satellite's 360 MHz transmissions. The original plan was to receive this beacon on a dipole antenna, but the satellite's transmissions on this frequency were somewhat weaker than predicted. The six-meter dish antenna (Figure 7) was used to track the satellite with considerable



FIGURE 7 - TRACKING ANTENNA (GREEN MOUNTAIN)

success, but other tracking commitments occasionally pre-empted its use. The system of nine element yagi antennas in Figure 8 was constructed and the receiver was switched from one antenna to the next as the satellite passed overhead. This scheme met with only limited success, and it was necessary to install a high gain preamplifier. This preamplifier was connected to an eight-turn helix antenna which was set at a fixed elevation but adjustable in azimuth. The twenty-two decibel gain in the helical antenna was sufficient to keep the 360 MHz receiver locked on the satellite's signal from horizon to horizon.

The polar orbit of the Beacon Explorer-B satellite brings it over the Huntsville location on a high elevation pass (above 45°) once each twelve hours, while the more equatorial orbit of the Beacon Explorer-C satellite brings it over Huntsville on a high elevation pass on four consecutive orbits each twenty-four-hour period. During a typical twenty-four hours, the day time and night time pass with the highest elevation was recorded, and, on the occasions when the Beacon Explorer-C satellite passed overhead on three of four consecutive orbits during the transient conditions which exist in the ionosphere around sunrise or sunset, several additional passes were recorded.

An attempt was made to automate the data reduction by reading the desired information off the magnetic tapes directly into the computers

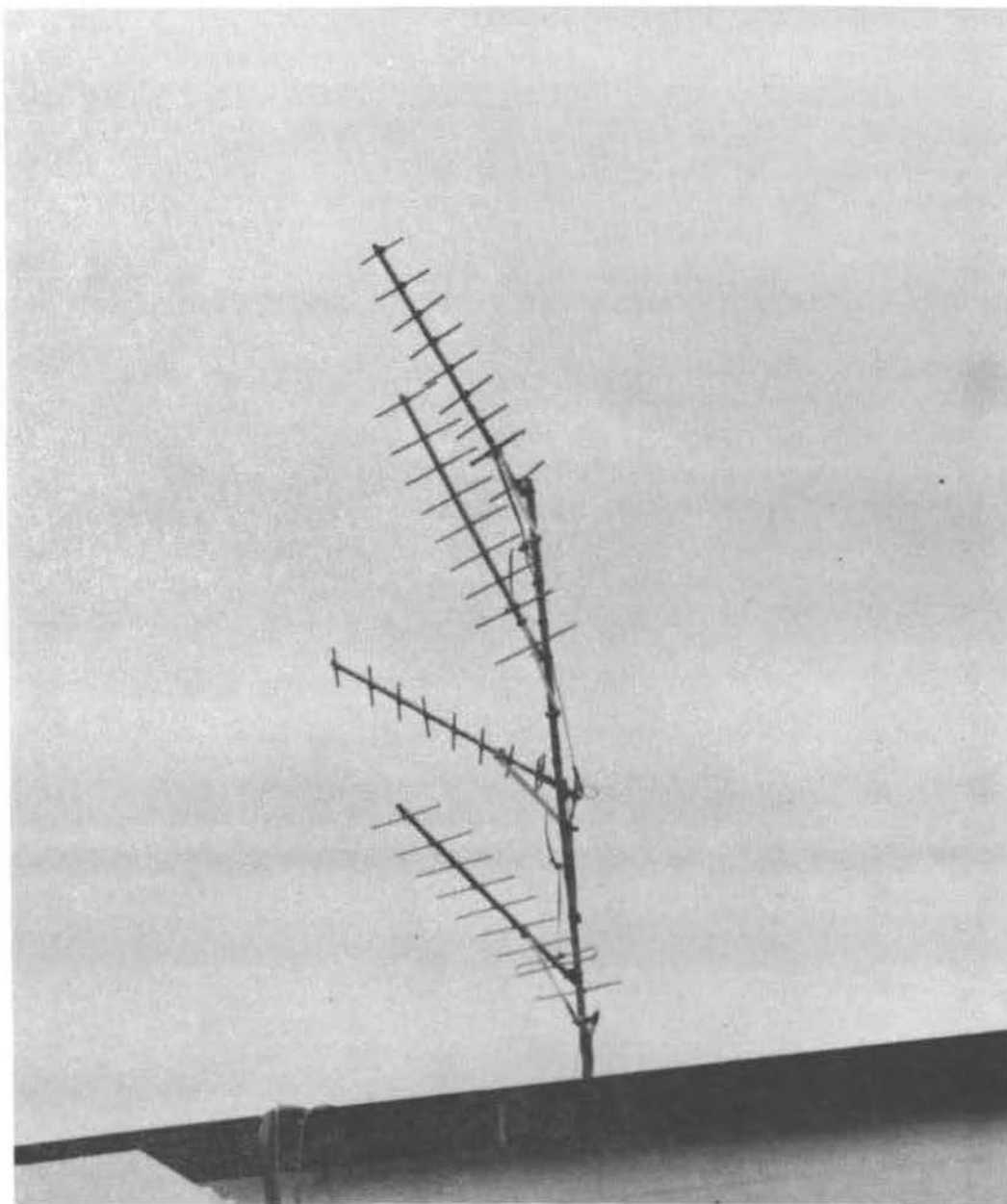


FIGURE 8 - 360-MHz YAGI ANTENNA SYSTEM

with automatic data processing equipment. It was discovered, however, that the slightest amount of noise on the tapes upset the machinery. When the technique was finally developed, it required a working time-to-data time ratio of over thirty to one, and so was abandoned.

The large amount of data received by the Green Mountain Station was reduced by undergraduate students from the Alabama Agricultural and Mechanical College. In reducing a recorded pass, the data channels were paired, with the 20-MHz Faraday rotation channel being reduced together with the 20- and 360-MHz dispersive Doppler channel and the 40-MHz Faraday rotation channel being reduced together with the 40- and 360-MHz dispersive Doppler channel. The times of two adjacent signal level nulls were read from the Faraday rotation channel and the number of dispersive Doppler cycles between the two times was counted. The data were then tabulated in a form which was acceptable by the digital computers at MSFC which evaluated it for electron content.

The recording chart speed was five millimeters a second and it was possible to determine the time of each signal level minimum to within two-tenths of a second and the number of dispersive Doppler cycles in an interval to within one-half cycle. An increase in chart speed would not have increased the accuracy substantially, as the background noise often made the exact position of the signal level minima uncertain by one or two tenths of a second.

III. MAGNETO-IONIC THEORY

The ionosphere is that region of the upper atmosphere which is characterized by a relatively high density of free electrons. The region extends from approximately sixty to one-thousand kilometers above the surface of the earth and the electron density distribution is approximately a parabolic function of height with a maximum at about three-hundred kilometers. The geomagnetic field influences the entire region [3].

The use of transmissions from earth satellites to analyze the ionosphere requires the development of a theory which relates the presence of free electrons to the propagation of radio waves. A complete mathematical analysis of the theory of the propagation of radio waves in the ionosphere would require a full wave theory treatment of considerable complexity. It is possible, however, to make a few assumptions about the ionosphere itself which greatly simplify the problem.

Thus, the ionosphere is considered to be a partially ionized, homogeneous gas made up of free electrons, heavy positive ions and heavy neutral molecules. It will be assumed that the medium as a whole is electrically neutral and subjected to a uniform, external magnetic field. The medium just defined is called a magneto-ionic medium and the theory

is called the magneto-ionic theory [4]. In most cases, it is possible to assume the ionosphere to be well represented by a magneto-ionic medium and obtain results which are consistent with experimental observations made by other means.

A. The Appleton-Hartree Equation

If a sinusoidal electromagnetic wave is traveling through a magneto-ionic medium with an electric field $\vec{E} = \vec{E}_0 e^{i\rho(\omega t)}$, it will subject a single free electron to the force, $+eE$ (where e is the magnitude of the charge of the electron). The force exerted by the magnetic field of the wave can be neglected; however, the magnetic field imposed upon the medium exerts a force of $e\dot{\vec{r}} \times \vec{B}$ on the electron. If the electron makes ν collisions per second with other particles, then it will be subjected to a damping force of $\nu m \dot{\vec{r}}$. Thus, the equation of motion of the electron is

$$m \ddot{\vec{r}} = -e\vec{E} - e\dot{\vec{r}} \times \vec{B} - \nu m \dot{\vec{r}} \quad (1)$$

It is convenient at this point to replace the electron displacement with an equivalent dipole moment, $\vec{p} = -e\vec{r}$. The equation of motion becomes

$$\ddot{\vec{p}} + \frac{e}{m} \dot{\vec{p}} \times \vec{B} + \nu \dot{\vec{p}} = \frac{e^2}{m} \vec{E} \quad (2)$$

It is possible to extend this equation to the case of a continuous charge distribution and average it over a finite region of space by introducing the concept of a dipole moment per unit volume, $\vec{P} = -Ne\vec{r}$,

where N is the electron density. This results in the following equation:

$$\ddot{\vec{P}} + \frac{e}{m} \dot{\vec{P}} \times \vec{B} + \nu \dot{\vec{P}} = \frac{Ne^2}{m} \vec{E} \quad (3)$$

In solving this equation, it is generally assumed that \vec{P} varies with \vec{E} , that is, $\vec{P} = \vec{P}_0 \exp(j\omega t)$. Substituting this expression into Eq. (3) gives

$$\frac{Ne^2}{m\omega^2} \vec{E} = (j\frac{\nu}{\omega} - 1) \vec{P} + j\frac{e}{m\omega} \vec{P} \times \vec{B} \quad (4)$$

This equation is called the "constitutive relation" of the ionosphere. Rewriting it in the more convenient notation which was introduced by Appleton, the equation becomes

$$\epsilon_0 \vec{\Sigma} \vec{E} = (jZ - 1) \vec{P} + j \vec{P} \times \vec{Y} \quad (5)$$

where

$$\begin{aligned} \Sigma &= \frac{Ne^2}{\epsilon_0 m \omega^2} \\ Y &= \frac{e}{m\omega} B \\ Z &= \frac{\nu}{\omega} \end{aligned}$$

It is now necessary to consider the electromagnetic wave itself. The electromagnetic field of the wave is governed by the four equations of Maxwell and a solution must satisfy these equations as well as the constitutive relation. In the case of the ionosphere, Maxwell's equations are simplified since it is assumed that there is no charge density and no

net current density. With these conditions and the relation $\vec{D} = \epsilon_0 \vec{E} + \vec{P}$, the equations become [5]

$$\nabla \cdot (\epsilon_0 \vec{E} + \vec{P}) = 0 \quad (6)$$

$$\nabla \cdot \vec{H} = 0 \quad (7)$$

$$\nabla \times \vec{H} = \frac{\partial}{\partial t} (\epsilon_0 \vec{E} + \vec{P}) \quad (8)$$

$$\nabla \times \vec{E} = -\mu_0 \frac{\partial \vec{H}}{\partial t} \quad (9)$$

For present purposes, it is sufficient to consider the special case of a plane wave. It is then possible to simplify the equations further. If the z-axis is chosen to be the direction of propagation, then all of the components of \vec{E} and \vec{H} will vary with z, e.g., $\exp(-jkz)$, but will not vary in the x and y direction. Under this restriction, Eqs. (8) and (9) reduce to

$$jkH_y = j\omega(\epsilon_0 E_x + P_x) \quad (10a)$$

$$-jkH_x = j\omega(\epsilon_0 E_y + P_y) \quad (10b)$$

$$0 = j\omega(\epsilon_0 E_z + P_z) \quad (10c)$$

$$jkE_y = -j\omega\mu_0 H_x \quad (11a)$$

$$jkE_x = -j\omega\mu_0 H_y \quad (11b)$$

with all other components zero.

Equations (5), (10), and (11) are sufficient to completely analyze the propagation in a homogeneous ionosphere of a plane wave with otherwise arbitrary polarization. In general, this polarization will change as the wave propagates; however, there exist certain polarizations which do not change. An electromagnetic wave possessing this property is known as a "characteristic wave."

In order to determine what types of polarization will propagate as characteristic waves, it is necessary to define the polarization of a wave in terms of the complex ratios $\frac{E_y}{E_x}$, $\frac{E_z}{E_x}$, $\frac{H_y}{H_x}$, and $\frac{H_z}{H_x}$. In a characteristic wave, these ratios remain constant.

Now, combining Eqs. (10a) and (11b), and Eqs. (10b) and (11a) gives

$$\frac{k^2}{\epsilon_0 \mu_0 \omega^2} = 1 + \frac{1}{\epsilon_0} \frac{P_x}{E_x} \quad (12a)$$

$$\frac{k^2}{\epsilon_0 \mu_0 \omega^2} = 1 + \frac{1}{\epsilon_0} \frac{P_y}{E_y} \quad (12b)$$

It follows that

$$\frac{P_x}{P_y} = \frac{E_x}{E_y} \quad (13)$$

It is possible to determine the ratio $\frac{P_x}{P_y}$ in terms of macroscopically observable parameters, but first it is necessary to define a coordinate system. The z-axis has already been chosen to be the direction of propagation, but there is still some freedom in the choice

of the direction of the x- and y-axis. If the y-axis is chosen so that the imposed magnetic field is in the y-z plane, the components of Eq.

(5) can be simplified somewhat. These components are

$$\epsilon_0 \Sigma E_x = (jZ-1)P_x + jP_y Y_L - jP_z Y_T \quad (14a)$$

$$\epsilon_0 \Sigma E_y = (jZ-1)P_y - jP_x Y_L \quad (14b)$$

$$\epsilon_0 \Sigma E_z = (jZ-1)P_z + jP_x Y_T \quad (14c)$$

where $Y_L = Y_z = |\vec{Y}| \cos \theta$
 $Y_T = Y_y = |\vec{Y}| \sin \theta$

and θ is the angle measured from the magnetic field to the wave normal.

Combining Eqs. (10c) and (14c) gives

$$P_z = \frac{Y_T}{1-jZ-\Sigma} P_x \quad (15)$$

Using Eq. (15) to eliminate P_z from Eq. (14a) gives

$$\epsilon_0 \Sigma \frac{E_x}{P_x} = -\left(1-jZ - \frac{Y_T^2}{1-jZ-\Sigma}\right) + j \frac{P_y}{P_x} Y_L \quad (16)$$

From Eqs. (13) and (14b)

$$\epsilon_0 \Sigma \frac{E_x}{P_x} = -(1-jZ) - j \frac{P_x}{P_y} Y_L \quad (17)$$

Equating the right-hand sides of Eqs. (16) and (17) results in

$$j Y_L \left(\frac{P_x}{P_y} \right) - \left(\frac{Y_T^2}{1-jZ-\Sigma} \right) + j Y_L \left(\frac{P_y}{P_x} \right) = 0 \quad (18)$$

Multiplying by $\left(\frac{P_x}{P_y}\right)$ gives the quadratic equation

$$\left(\frac{P_x}{P_y}\right)^2 + \frac{j}{Y_L} \left(\frac{Y_T^2}{1-jZ-X} \right) \frac{P_x}{P_y} + 1 = 0 \quad (19)$$

whose solution is

$$R = \left(\frac{P_x}{P_y}\right) = \left(-\frac{j}{Y_L}\right) \left[\frac{\frac{1}{2} Y_T^2}{1-jZ-X} \mp \left(\frac{\frac{1}{4} Y_T^4}{[1-jZ-X]^2} + Y_L^2 \right)^{1/2} \right] \quad (20)$$

This equation is called the "polarization equation" and a wave propagating within the ionosphere must have a polarization given by one of its two solutions. In general, R is complex, corresponding to elliptical polarization. The two limiting cases, R real and R imaginary, correspond to linear and circular polarizations, respectively.

In order to complete the treatment of propagation within a homogeneous ionosphere, it is necessary to develop an expression for the index of refraction of the medium. Recalling Eq. (12b), and that $v = \frac{\omega}{k}$, $c = \frac{1}{\mu_0 \epsilon_0}$, and $n = \frac{c}{v}$, then

$$n^2 = 1 - \frac{1}{\epsilon_0} \frac{P_x}{E_y} \quad (21)$$

where n is the index of refraction. From Eq. (14b), it is seen that

$$\frac{P_x}{E_y} = - \frac{\epsilon_0 X}{1-jZ + j\left(\frac{P_x}{P_y}\right) Y_L} \quad (22)$$

Combining Eqs. (21) and (22) gives

$$n^2 = 1 - \frac{X}{1-jZ + j\left(\frac{P_x}{P_y}\right) Y_L} \quad (23)$$

The term $\left(\frac{P_x}{P_y}\right)$, the polarization of the wave, has already been evaluated in Eq. (20). Introducing this term into Eq. (23) gives

$$n^2 = 1 - \frac{X}{1 - jZ - \frac{\frac{1}{2}Y_T^2}{1 - jZ - X} \pm \left[\frac{\frac{1}{4}Y_T^4}{(1 - jZ - X)^2} + Y_L \right]^{1/2}} \quad (24)$$

This formula, known as the Appleton-Hartree equation, is a major tool in the study of the ionosphere by means of radio wave propagation. Recalling that the equation was derived for a continuous medium, it is to be noted that the equation is strictly valid only for homogeneous regions in the ionosphere; however, its successful application to a variety of problems has proved to be quite representative of the actual ionosphere.

An examination of the equation indicates that the ionosphere possesses very complicated optical properties. The geomagnetic field makes the ionosphere an anisotropic medium similar to a biaxial crystal, and produces the two indices of refraction of Eq. (24).

The two solutions of Eq. (24) are the refractive indices for the so-called ordinary and extraordinary modes of propagation.

B. Approximations to the Appleton-Hartree Equation

In its entirety, the Appleton-Hartree equation is rather cumbersome to work with due to its complicated dependence upon the electron density and the earth's magnetic field. It is possible to simplify the equation considerably by placing a few restrictions on it.

The first approximation assumes that the electron collision frequency is small (i. e., $Z \ll 1$) and introduces very little error at higher frequencies, particularly in the middle or upper regions of the ionosphere.

By restricting the use of the equation to regions of the ionosphere where the angle between the magnetic field and the ray path (angle Θ) is small, it is possible to utilize the quasi-longitudinal (Q-L) approximation. This approximation is valid (above 20 MHz) for an observer of the ionosphere at mid-latitudes in the northern hemisphere, except for a small region of the sky to the north. When the condition of the approximation is realized, then

$$\frac{Y_T^4}{Y_L^2} \ll (1-X)^2 \quad (25)$$

Applying both of these approximations to Eq. (24), the Appleton-Hartree equation becomes

$$n^2 = 1 - \frac{X}{1 \pm Y_L} \quad (26)$$

The ordinary and extraordinary refractive indices are then given by

$$\mu_o = \left[1 - \frac{\Sigma}{1 + Y_L} \right] \quad (27)$$

$$\mu_e = \left[1 - \frac{\Sigma}{1 - Y_L} \right] \quad (28)$$

where the symbol μ has been used in keeping with standard notation.

In several applications, it is possible to neglect the geomagnetic field altogether and treat the ionosphere as if it were an isotropic medium. In such cases, the isotropic refractive index is given by

$$\mu = \left[1 - \Sigma \right]^{\frac{1}{2}}. \quad (29)$$

C. Propagation in an Anisotropic Medium

The analysis of radio wave propagation within the ionosphere would be greatly simplified if it were possible to neglect the anisotropic properties of the region. However, since it is these properties which are responsible for the Faraday rotation effect, it is necessary to study them in detail.

In the ionosphere, the refractive index depends upon the angle between the magnetic field and the wave normal, but when tracing the path of a ray through an interface between two regions of different refractive indices, the direction of the wave normal in the second region cannot be determined unless the index of refraction of the second region is already known. In addition, the ray direction (direction of Poynting's vector) does not coincide with the wave normal and, in general, does not remain in the plane of incidence [6] .

The relation between the ray direction and the direction of the wave normal can be determined with the aid of Figure 9. This figure is an approximate plot of the "wave-velocity" surfaces ($\frac{1}{\mu}$) of the ordinary and extraordinary modes of propagation using Eqs. (27) and (28). The figure is actually a surface of revolution about the magnetic field vector. If a disturbance originates at O , then each surface represents the wave front after some time τ . At the point S , the wave

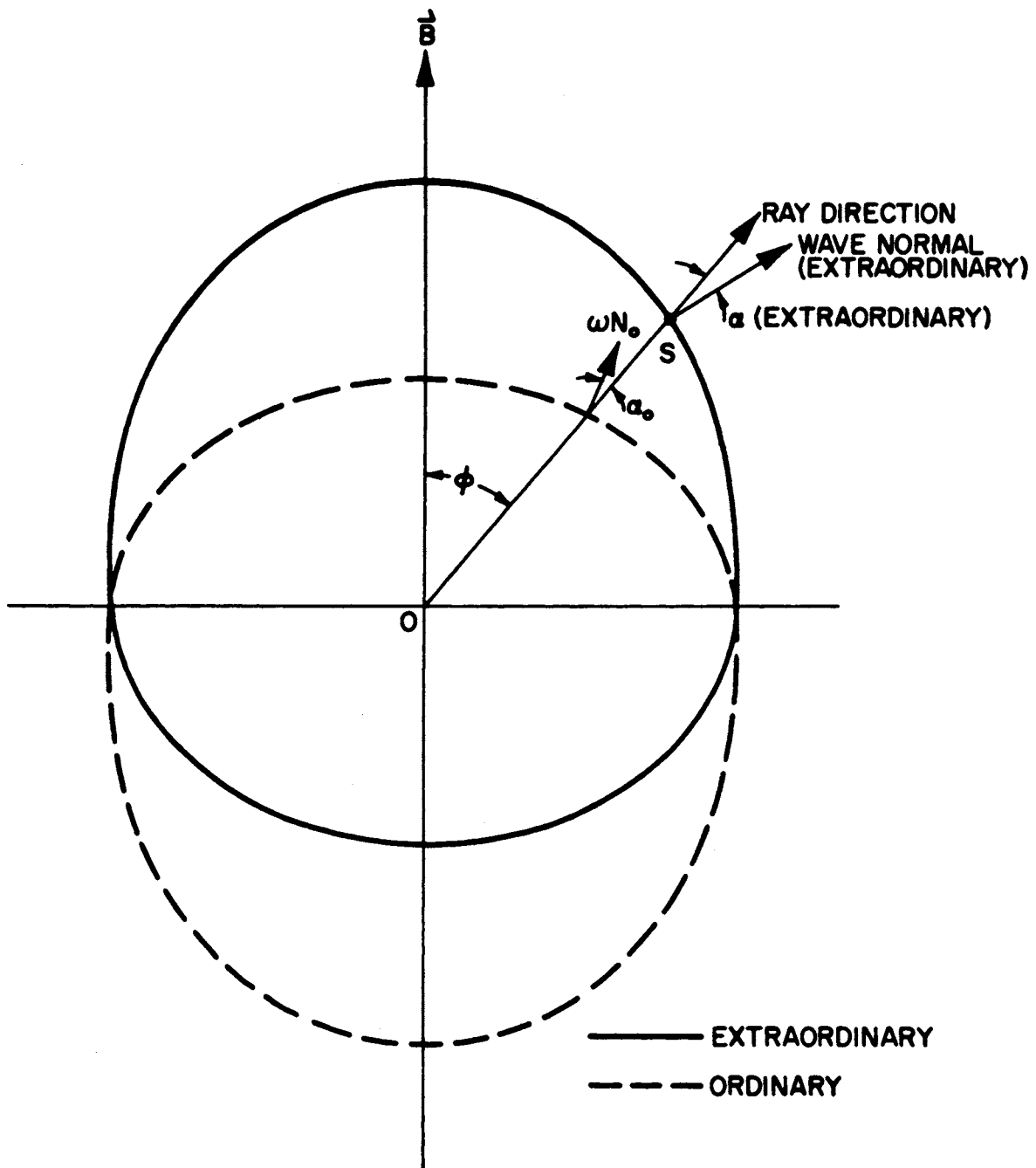


FIGURE 9 - WAVE VELOCITY SURFACES ($\frac{1}{\mu}$)

front is traveling in the direction normal to the surface and obviously not radially. Since the energy which is arriving at the point S is traveling from the point O , it is apparent that in an anisotropic medium, the direction of phase propagation differs, in general, from that of energy propagation. From the figure, it is seen that both the ordinary and extraordinary rays lie in the plane defined by their wave normals and the magnetic field, but for $-\frac{\pi}{2} < \phi < \frac{\pi}{2}$ the direction of the extraordinary ray is such that it lies between its wave normal and the magnetic field, while the opposite is true for the ordinary ray.

At this point, it will be appropriate to introduce the concept of a ray velocity (v_r) which will be defined as the phase velocity in the direction of the energy flow. The velocity of the point S , given by the expression $v = \frac{c}{\mu}$ is the phase velocity in the direction of the wave normal. It is seen that the phase velocity in the direction of the ray is given by

$$v_r = \frac{v}{\cos \alpha} \quad (30)$$

It is also interesting to consider the phase path length (the distance the wave would travel in time τ if it were in free space) in an anisotropic medium. In traveling the distance d , the wave takes a

time

$$\tau = \frac{d}{v_r} \quad (31)$$

From Eqs. (30) and (31) and the definition of the index of refraction,

$$\tau = \frac{(\mu \cos \alpha) d}{c} \quad (32)$$

If the distance traveled by the wave in free space in time τ is P ,

then

$$\tau = \frac{P}{c} \quad (33)$$

and combining Eqs. (32) and (33) gives for the phase path length

$$P = (\mu \cos \alpha) d \quad (34)$$

It is possible to determine the relation between the refractive index and the angle α by referring to Figure 10. From the geometry of the figure and the sign convention that the angle θ is positive when measured to the wave normal in the same sense as the angle α , it is seen that

$$\tan \alpha = -\frac{1}{r} \frac{dr}{d\theta} \quad (35)$$

and

$$\theta = \theta - \alpha \quad (36)$$

Combining Eqs. (30), (35), and (36) gives

$$\tan \alpha = -\frac{1}{v} \frac{dv}{d\theta} = \frac{1}{\mu} \frac{d\mu}{d\theta} \quad (37)$$

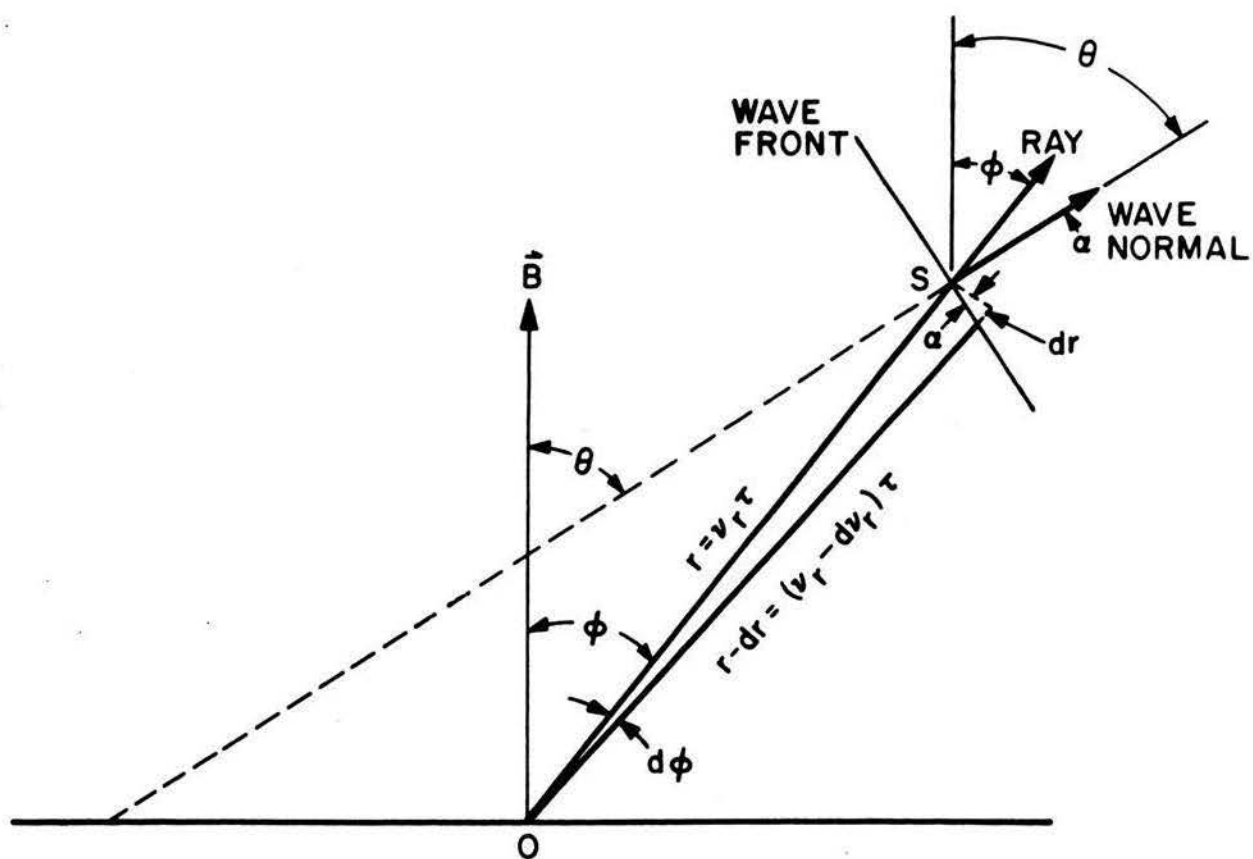


FIGURE 10 - GEOMETRY FOR CALCULATING α

When this relation is combined with the full Appleton-Hartree equation ($Z=0$) the results are

$$\tan \alpha = \pm \frac{(n^2 - 1) Y_T Y_L}{[Y^4 + 4(1 - X) Y_L^2]^{1/2}} \quad (38)$$

where the plus and minus signs refer to the ordinary and extraordinary ray, respectively. Applying the quasi-longitudinal approximation reduces the equation to

$$\tan \alpha = \mp \frac{XY \sin \theta}{2(1 - X)(1 \pm Y \cos \theta)} \quad (39)$$

D. The Faraday Rotation Effect

To consider the problem of propagation of a linearly polarized electromagnetic wave in the ionosphere, it will be necessary to return to Eq. (20), the polarization equation. If the quasi-longitudinal approximation is applied to this expression, then $R = \pm j$, indicating that under this condition there are two characteristic waves (both circularly polarized, but with different senses of rotation). Since these two circularly polarized waves are the components of a single linearly polarized wave, it would appear that a linearly polarized wave is also a characteristic wave. A closer examination, however, shows that this is not strictly true because the ratio $R = \frac{E_x}{E_y}$ does not remain constant.

To determine the effect of the ionosphere upon R for a linearly polarized wave [7], consider such a wave propagated at $t=0$ and $z=0$ with its electric vector along the y-axis (i. e., $E_x=0$). The x and y components of each circularly polarized wave are related to the x and y components of the linearly polarized wave by

$$E_x = E_{x0} + E_{xe} \quad (40a)$$

$$E_y = E_{y0} + E_{ye} \quad (40b)$$

where the 0 and e subscripts refer to the ordinary and extraordinary modes of the circularly polarized waves.

These circular components each vary with z and t as

$$E_{x_0} = E_{x_0} \exp[j(\omega t - k_0 z_0)] \quad (41a)$$

$$E_{x_e} = E_{x_e} \exp[j(\omega t - k_e z_e)] \quad (41b)$$

$$E_{y_0} = E_{y_0} \exp[j(\omega t - k_0 z_0)] \quad (41c)$$

$$E_{y_e} = E_{y_e} \exp[j(\omega t - k_e z_e)] \quad (41d)$$

In these expressions z_0 and z_e have been included to allow for the possibility that the ordinary and extraordinary rays may follow separate paths. For brevity, the term $\cos \alpha$ is contained implicitly in the definition of the refractive index in the remainder of this section.

At the initial conditions,

$$E_{x_1} = E_{x_0} + E_{x_e} = 0 \quad (42a)$$

$$E_{y_1} = E_{y_0} + E_{y_e} \quad (42b)$$

and R is initially zero for the linearly polarized wave.

Equation (40) may be rewritten as

$$E_x = R_0 E_{y_0} + R_e E_{y_e} \quad (43a)$$

$$E_y = E_{y_0} + E_{y_e} \quad (43b)$$

where R_0 and R_e now refer to the polarization of the two circular waves.

Thus,

$$R = \frac{E_x}{E_y} = \frac{R_o E_{y_o} \exp(-j k_o z_o) + R_e E_{y_e} \exp(-j k_e z_e)}{E_{y_o} \exp(-j k_o z_o) + E_{y_e} \exp(-j k_e z_e)} \quad (44)$$

Rewriting Eq. (42) as

$$E_{x_1} = R_o E_{y_o} + R_e E_{y_e} = 0$$

$$E_{y_1} = E_{y_o} + E_{y_e}$$

and recalling that $R_o = -j$ and $R_e = j$ indicates that

$$E_{y_o} = \frac{E_{y_1}}{2} \quad (45a)$$

$$E_{y_e} = \frac{E_{y_1}}{2} \quad (45b)$$

Substituting Eq. (45) and $R = \pm j$ into Eq. (44) gives

$$R = \frac{-j \exp(-j k_o z_o) + j \exp(-j k_e z_e)}{\exp(-j k_o z_o) + \exp(-j k_e z_e)} \quad (46)$$

Multiplying the numerator and denominator of Eq. (46) by $j \exp[\frac{j}{2}(k_o z_o + k_e z_e)]$ gives

$$R = \frac{\exp[-\frac{j}{2}(k_o z_o - k_e z_e)] - \exp[\frac{j}{2}(k_o z_o - k_e z_e)]}{j \exp[-\frac{j}{2}(k_o z_o - k_e z_e)] + j \exp[\frac{j}{2}(k_o z_o - k_e z_e)]} \quad (47)$$

Defining the quantity $\beta = \frac{1}{2}(k_o z_o - k_e z_e)$ and substituting into Eq. (47) gives

$$R = \frac{1}{j} \frac{\exp(-j\beta) - \exp(j\beta)}{\exp(-j\beta) + \exp(j\beta)} \quad (48)$$

Now, comparing Eq. (48) with the identity

$$\tan \beta = \frac{1}{j} \frac{\exp(j\beta) - \exp(-j\beta)}{\exp(j\beta) + \exp(-j\beta)}$$

indicates that $R = -\tan \beta$. Thus, after traveling a distance z within the ionosphere, the quantity R remains real, indicating the wave has retained its linear polarization; but R has changed in magnitude by an amount $\tan \beta$. Recalling that $R = \frac{E_x}{E_y}$, it is apparent that the plane of polarization has rotated an angle β , where

$$\beta = \frac{1}{2} (k_o z_o - k_e z_e) \quad (49)$$

Since $k = \frac{2\pi}{\lambda} n$, it is possible to express the angle β in terms of the solutions of the Appleton-Hartree equation. Thus, $\beta = \frac{\pi}{\lambda} (\mu_o z_o - \mu_e z_e)$. Dividing the rotation angle by 2π to get the total number of rotations after the wave has propagated a distance z gives

$$\Omega = \frac{\beta}{2\pi} = \frac{f}{2c} (\mu_o z_o - \mu_e z_e) \quad (50)$$

For the actual case of propagation through the ionosphere, it is necessary to go to the integral form of the equation since μ_o and μ_e are continuously changing functions. Thus,

$$\Omega = \frac{f}{2c} \int \mu_o ds_o - \frac{f}{2c} \int \mu_e ds_e \quad (51)$$

where the integration is along the separate ray paths, ds_o and ds_e .

Since subsequent derivations will be in terms of phase path length differences, it will be convenient at this point to express the above Faraday rotation formula in terms of the phase paths. Equation (51) becomes

$$\Omega = \frac{f}{2c} (P_o - P_e) \quad (52)$$

where $P_o = \int \mu_o ds_o$ is the phase path length of the ordinary mode and $P_e = \int \mu_e ds_e$ is the phase path length of the extraordinary mode.

Several authors [8] have developed an approximate expression for the Faraday rotation angle which demonstrates the effect of the various parameters somewhat better than does Eq. (51). They assume a common ray path for the two modes of propagation and combine Eqs. (27), (28), and (51) to get

$$\Omega = \frac{f}{2c} \int \left[\left(1 - \frac{\Sigma}{1+\gamma_k} \right)^{\frac{1}{2}} - \left(1 - \frac{\Sigma}{1-\gamma_k} \right)^{\frac{1}{2}} \right] dz$$

Expanding the terms under the square root sign as a power series and dropping the higher order terms gives

$$\Omega = \frac{f}{2c} \int \left[\frac{\Sigma}{2} \left(\frac{1}{1-\gamma_k} - \frac{1}{1+\gamma_k} \right) \right] dz$$

Expanding the fractions in terms of a series and again dropping the higher order terms gives

$$\Omega = \frac{f}{2c} \int \Sigma \gamma_k dz$$

Recalling the definition of Σ and γ_k reduces the expression to

$$\Omega = \frac{k}{f^2} B \cos \theta \int N dz \quad (53)$$

where

$$k = \frac{e^3}{16\pi^2 c \epsilon_o m^2}$$

The term $\int N dz$ is interpreted as the total ionization along the ray path. Although Eq. (53) is only an approximate solution to the problem, it has been used frequently with some success.

E. The Dispersive Doppler Effect

The dispersive Doppler effect arises from relative changes in the phase path length of two transmissions from the moving satellite [9] . This phase path length is defined as

$$P_f = \int_0^{R_s} \mu_f ds \quad (54)$$

where μ_f is the refractive index of the ionosphere at frequency f

R_s is the range to the satellite

ds is along the ray path.

As the satellite passes over the receiver, the phase path length will change with time. This time rate of change is due to changes in both the range to the satellite and the refractive index itself. Rewriting Eq. (54) to show its dependence on the various parameters gives

$$P_f(R_s, t) = \int_0^{R_s} \mu_f(s, t) ds \quad (55)$$

since μ is a function of the height above the earth. The time derivative of Eq. (55) is

$$\frac{dP}{dt} = \frac{\partial P}{\partial t} + \frac{\partial P}{\partial R_s} \frac{\partial R_s}{\partial t} \quad (56)$$

where

$$\frac{\partial P}{\partial t} = \int_0^{R_s} \left(\frac{\partial \mu_f}{\partial t} \right) ds \quad (57)$$

$$\frac{\partial P}{\partial R_s} = (\mu_f)_{R_s} \quad (58)$$

and $(\mu_f)_{R_s}$ is the refractive index evaluated at the position of the satellite and at frequency f . For present purposes, it will be possible to assume the satellite is in free space (i.e., above the ionosphere) and set $(\mu_f)_{R_s}$ equal to one.

Combining Eqs. (56), (57), and (58) gives

$$\frac{dP}{dt} = \frac{dR_s}{dt} + \int_0^{R_s} \left(\frac{\partial \mu_f}{\partial t} \right) ds \quad (59)$$

Recalling that the time rate of change in the phase of a wave is

$$\frac{d\phi}{dt} = \frac{2\pi f}{c} \frac{dP}{dt} \quad (60)$$

and the frequency seen by the receiver is equal to the transmitted frequency plus $\left(\frac{1}{2\pi}\right)$ times the rate of change of the phase, then

$$f' = f + \frac{f}{c} \frac{dR_s}{dt} + \frac{f}{c} \int_0^{R_s} \left(\frac{\partial \mu_f}{\partial t} \right) ds \quad (61)$$

where f' is the received frequency.

Examining the right-hand side of Eq. (61), it is seen that the second term is just the ordinary Doppler shift frequency. The third term is a slight additional change in the received frequency and has become known as the "Doppler shift offset."

It is possible to eliminate the regular Doppler shift by transmitting a second wave of frequency mf , in phase with the first. The frequency observed by the receiver of this second wave is

$$f'' = mf + \frac{mf}{c} \frac{dR_s}{dt} + \frac{mf}{c} \int_0^{R_s} \left(\frac{\partial \mu_{mf}}{\partial t} \right) ds \quad (62)$$

If the frequency of the second transmission is divided by the factor m upon reception and then subtracted from the first frequency, the observed beat frequency will be

$$F = \frac{f}{c} \int_0^{R_s} \left(\frac{\partial \mu_f}{\partial t} \right) ds_f - \frac{f}{c} \int_0^{R_s} \left(\frac{\partial \mu_{mf}}{\partial t} \right) ds_{mf} \quad (63)$$

where it must be remembered that the integrations are along the separate ray paths.

Since the ionosphere is a highly dispersive medium, the beat frequency is readily observable if m is as small as two; however, since the frequency is often less than a cycle per second and changing rapidly, it is impossible to determine it accurately from transcribed records. In order to utilize the effect it is necessary to resort to finite time intervals and consider the total change in phase during this interval. In this case, the expression for the dispersive Doppler effect becomes the Eq. (63)

$$F \Delta t = \frac{f}{c} \int_{t_1}^{t_2} \mu_{mf} ds_{mf} - \frac{f}{c} \int_{t_1}^{t_2} \mu_f ds_f - \frac{f}{c} \int_{t_1}^{t_2} \mu_{mf} ds_{mf} + \frac{f}{c} \int_{t_1}^{t_2} \mu_f ds_f \quad (64)$$

where t_1 and t_2 indicate a change in the geometry.

In terms of the respective phase path lengths, Eq. (64) may be written

$$F \Delta t = \frac{f}{c} \Delta (P_{mf} - P_f) \quad (65)$$

It will be noted that in going from Eq. (63) to Eq. (64) the free space Doppler shift was reintroduced into each term, but in calculations using Eq. (64) these extraneous terms will cancel one another.

IV. THE RAY PATH LENGTH FOR OBLIQUE INCIDENCE IN IN A SPHERICALLY STRATIFIED IONOSPHERE

Equations (52) and (65) are exact expressions for the Faraday rotation and dispersive Doppler effects, but the implicit ray path lengths have not yet been defined. The problem is easily solved by assuming that the ray paths coincide with the straight line between the receiving station and the satellite, but this is not realistic. For instance, the most easily observed parameter of the ray path, the angle of arrival of the satellite's transmissions, can vary (at 20 MHz) more than ten degrees from the actual elevation of the satellite.

To develop an expression for the ray path length as a function of the position of the satellite, it is necessary to assume the ionosphere to be a completely known quantity. This, of course, defeats the purpose of the entire analysis and will require further discussion. In addition, it will be assumed that whatever the distribution of electrons within the ionosphere it is a function of only the height above the surface of the earth (i. e., spherically stratified and ephemeris time). Although it would be possible to remove these last two conditions, they are quite plausible and the refinement would not justify the required effort.

A. The Isotropic Ray Path

Since the dispersive Doppler effect is a phenomenon which is dependent upon only the dispersive properties of the ionosphere, it will be possible, in its analysis, to assume the ionosphere to be an isotropic medium. In addition, it is somewhat simpler, mathematically, to assume that propagation is taking place from the station to the satellite.

The coordinate system is defined in Figure 11. The satellite will always be taken to be in the positive quadrant of the y - z plane which, it will be noted, is also the plane of incidence. It can be seen from the figure that

$$ds = \frac{dh}{\cos \chi} \quad (66)$$

$$ds = \frac{dh}{[1 - \sin^2 \chi]^{1/2}} \quad (67)$$

where χ is a continuously changing angle of incidence at the interfaces of the differential geocentric stratifications.

If the ionosphere is spherically stratified, then

$$\sin \chi = \left(\frac{R}{R+h} \right) \frac{\sin \chi_f}{\mu} \quad (68)$$

where

χ_f = the apparent zenith angle

R = the radius of the earth

μ = refractive index at height h

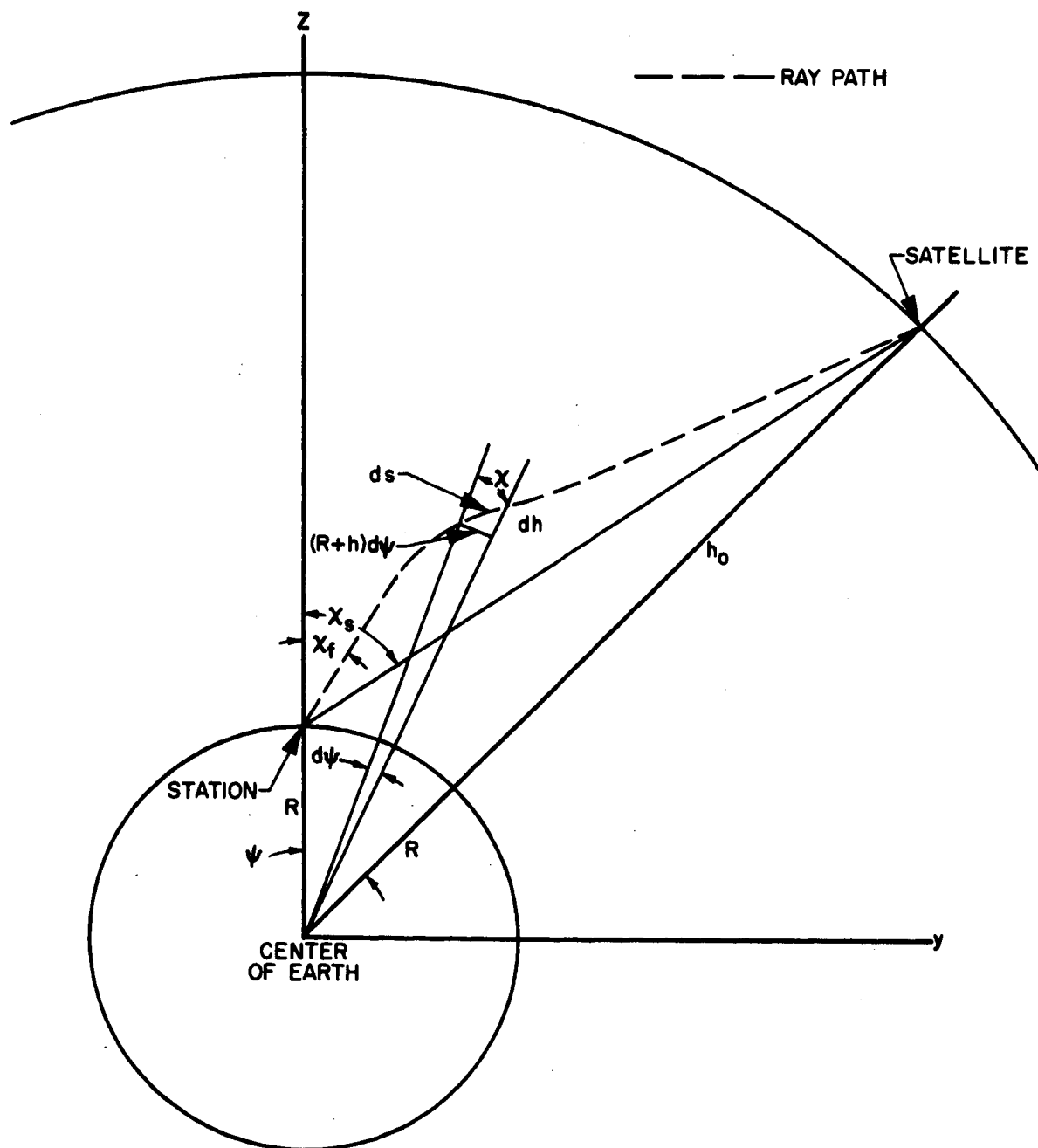


FIGURE 11 - GEOMETRY FOR THE RAY PATH

That this is true can be demonstrated with the aid of Figure

12. From the law of sines,

$$\sin \chi_f = \left(\frac{R+h_1}{R} \right) \sin \chi_1' \quad (69)$$

From Snell's law,

$$\sin \chi_1' = \mu_2 \sin \chi_2 \quad (70)$$

Applying the law of sines at the second layer gives

$$\sin \chi_2 = \left(\frac{R+h_1+h_2}{R+h_1} \right) \sin \chi_2' \quad (71)$$

Applying Snell's law a second time gives

$$\mu_2 \sin \chi_2' = \mu_3 \sin \chi_3 \quad (72)$$

From Eqs. (69) and (70),

$$\sin \chi_f = \mu_2 \left(\frac{R+h_1}{R} \right) \sin \chi_2 \quad (73)$$

From Eqs. (71), (72), and (73),

$$\sin \chi_f = \mu_3 \left(\frac{R+h_1+h_2}{R} \right) \sin \chi_3 \quad (74)$$

Since the increments of height between successive layers can be made arbitrarily small, then Eqs. (73) and (74) imply that Eq. (68) is true.

Substituting Eq. (68) into Eq. (67) gives

$$ds = \frac{\mu dh}{\left[\mu^2 - \left(\frac{R}{R+h} \right)^2 \sin^2 \chi_f \right]^{1/2}} \quad (75)$$

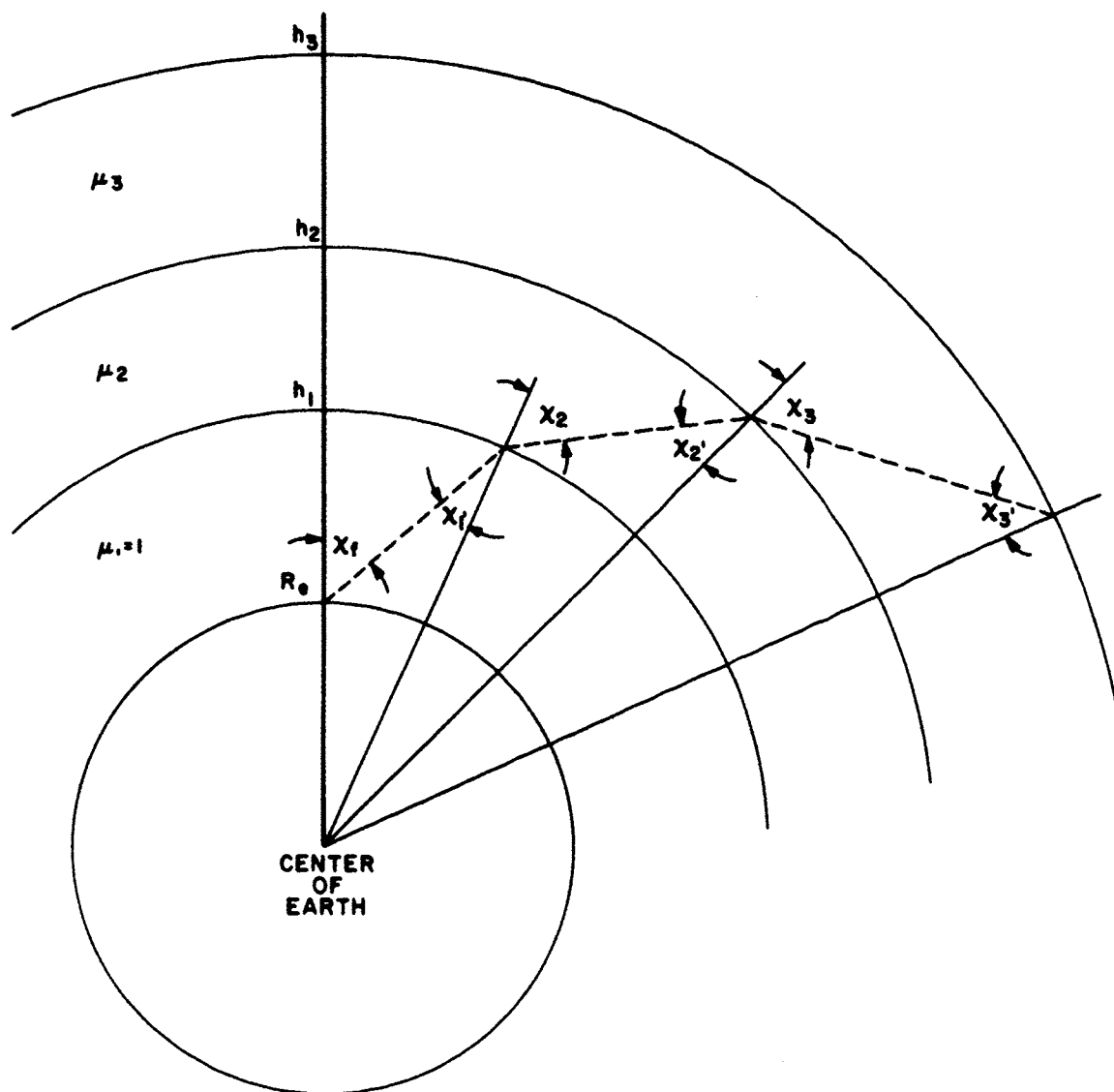


FIGURE 12 - BOUGUER'S RULE

Integrating this expression to the height of the satellite gives

$$S = \int_0^{h_s} \frac{\mu dh}{\left[\mu^2 - \left(\frac{R}{R+h} \right)^2 \sin^2 \chi_f \right]^{1/2}} \quad (76)$$

where χ_f is the "apparent" zenith angle of the satellite and μ is calculated according to Eq. (29).

For high elevation angles, it is possible to make the approximation $\chi_f = \chi_s$; however, this introduces a large error at elevation angles below about sixty degrees. To find the true value of χ_f , refer to Figure 11 and note that

$$\tan \chi = \frac{(R+h)d\psi}{dh} \quad (77)$$

Thus,

$$d\psi = \frac{\sin \chi dh}{(R+h) [1 - \sin^2 \chi]^{1/2}} \quad (78)$$

Recalling Equation 68 and integrating gives

$$\psi = \int \frac{R \sin \chi_f dh}{(R+h)^2 \left[\mu^2 - \left(\frac{R}{R+h} \right)^2 \sin^2 \chi_f \right]^{1/2}} \quad (79)$$

In the absence of an ionosphere μ will be unity along the ray path so the results of Equation (79) can also be obtained from the expression

$$\psi = \int_0^{h_s} \frac{R \sin \chi_s dh}{(R+h)^2 \left[1 - \left(\frac{R}{R+h} \right)^2 \sin^2 \chi_s \right]^{1/2}} \quad (80)$$

This equation can be integrated to give

$$\Psi = \text{Sin}^{-1} \left[\left\{ \left[1 - \left(\frac{R}{R+h_s} \right)^2 \text{sin}^2 \chi_s \right]^{1/2} - \left(\frac{R}{R+h_s} \right) \text{cos} \chi_s \right\} \text{sin} \chi_s \right] \quad (81)$$

By iterating the value of χ_f in Eq. (79) until its results agree with the results of Eq. (81), it is possible to obtain χ_f to any degree of accuracy consistent with the assumptions.

B. The Anisotropic Ray Path

The problem of determining the anisotropic ray path is much more complex and it is necessary to assume that the isotropic ray path is a good first approximation to the two anisotropic ray paths. This is justified by the results of detailed ray-tracing techniques [2] which show the ordinary and extraordinary ray paths to be virtually coincident along most of their length, even at very oblique angles of incidence.

The coordinate system to be used is the same as in the isotropic case and again the propagation will be assumed to be from the station to the satellite. In reversing the direction of propagation, the angle between the wave normal and the magnetic field is increased by 180 degrees. Although it can be seen from Figure 9 and Eqs. (27) and (28) that the effect of this is just to interchange the ordinary and extraordinary ray paths, it will be possible to retain the present definitions by mathematically reversing the magnetic field also.

The first quantity which must be determined in the calculation of the anisotropic ray path is the angle θ . Referring to Figure 11, the equation of the vector which extends from the center of the earth to a point of the ray path at height h is

$$\vec{N} = [(R+h) \sin \psi] \hat{j} + [(R+h) \cos \psi] \hat{k}$$

and the unit vector in this direction is given by

$$\hat{N} = \sin \psi \hat{j} + \cos \psi \hat{k} \quad (82)$$

Resorting to the approximation of coincident ray paths, the angle between the vector \hat{N} and the two anisotropic ray paths is given by Eq. (68), that is,

$$\chi = \sin^{-1} \left[\left(\frac{R}{R+h} \right) \frac{\sin \chi_f}{\mu} \right]$$

Thus, the unit vector in the direction of the ray paths becomes

$$\hat{S} = \sin(\psi + \chi) \hat{j} + \cos(\psi + \chi) \hat{k} \quad (83)$$

If the geomagnetic field (reversed) is given by

$$\vec{B} = B_x \hat{i} + B_y \hat{j} + B_z \hat{k}$$

then the angle between it and the wave normal at a point within the ionosphere can be calculated from the relation

$$\vec{B} \cdot \hat{S} = |\vec{B}| \cos \theta$$

Thus,

$$\cos \theta = \frac{B_y \sin(\psi + \chi) + B_z \cos(\psi + \chi)}{(B_x^2 + B_y^2 + B_z^2)^{\frac{1}{2}}} \quad (84)$$

With this angle determined, it is possible to calculate both the refractive index and the angle α for the ordinary and extraordinary modes of propagation. This information is enough to solve the problem, but caution must be exercised in the process. It will be recalled that,

in an anisotropic medium, it is the wave normal which obeys Snell's law and not the ray. The relation between the direction of the ray path and the wave normal and the geomagnetic field is shown in Figure 13. Letting \hat{S}_e be the unit vector in the direction of the extraordinary ray and \hat{W}_e the unit vector in the direction of the extraordinary wave normal, then

$$\hat{S}_e = \vec{o}\vec{a} + \vec{o}\vec{c} \quad (85)$$

where

$$\begin{aligned} \vec{o}\vec{a} &= |\vec{o}\vec{a}| \hat{W}_e \\ \vec{o}\vec{c} &= |\vec{o}\vec{c}| \hat{B} \\ \hat{W}_e &= \sin(\psi + \alpha_e) \hat{j} + \cos(\psi + \alpha_e) \hat{k} \end{aligned}$$

From the law of sines

$$\frac{|\vec{o}\vec{a}|}{\sin(\theta - \alpha_e)} = \frac{|\vec{o}\vec{c}|}{\sin \alpha_e} = \frac{l}{\sin \theta} \quad (86)$$

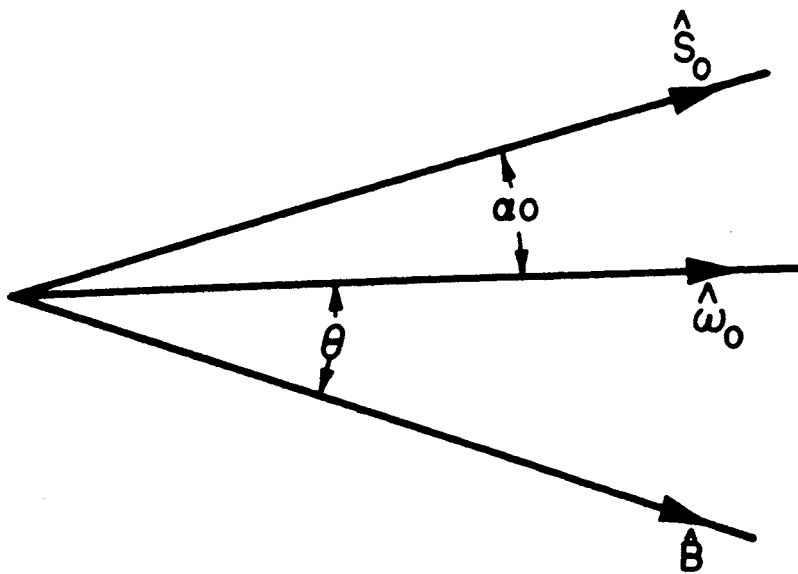
Combining Eqs. (85) and (86) gives

$$\hat{S}_e = \frac{\sin(\theta - \alpha_e)}{\sin \theta} \hat{W}_e + \frac{\sin \alpha_e}{\sin \theta} \hat{B} \quad (87)$$

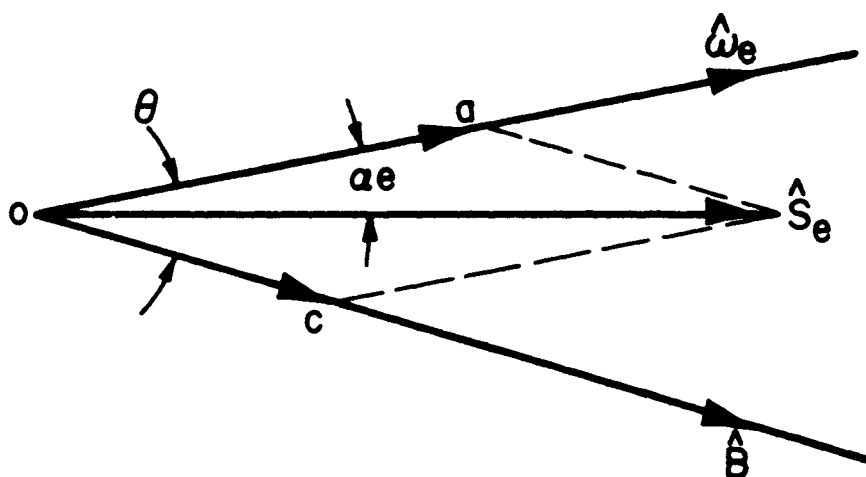
A similar procedure for the ordinary mode gives

$$\hat{S}_o = \frac{\sin(\theta + \alpha_o)}{\sin \theta} \hat{W}_o - \frac{\sin \alpha_o}{\sin \theta} \hat{B} \quad (88)$$

If the ray path did coincide with the wave normal and was not deflected through the angle α , it would be possible to find its length in the



(a) ORDINARY RAY DIRECTION



(b) EXTRAORDINARY RAY DIRECTION

height increment dh by the same equation which was used to find the isotropic path length. In this case, the height would be

$$ds'_e = \frac{dh}{\cos \chi_e} \quad (89)$$

$$ds'_o = \frac{dh}{\cos \chi_o} \quad (90)$$

where χ_o and χ_e are the angles of incidence of the ordinary and extraordinary wave normals at the spherical stratifications and the primes are to indicate that the quantities are not the ray path length.

It is possible, however, to relate the lengths ds'_o and ds'_e to the actual ray path lengths with Eqs. (87) and (88). Figure 14 shows the relation between the height increment, the ray path and the quantity given by Eq. (90). The more obvious method of relating the ray path increment to the height increment is through the angle between the unit vectors \hat{N} and \hat{S}_e . This however, leads to difficulties in obtaining the signs of the various angles. The difficulty can be avoided if an intermediate step is included. This intermediate step will be to first find the projection of ds_e on the y-z plane and then relate this projection to the quantity ds'_e .

The vector equation of the projection of \hat{S}_e onto the y-z plane can be obtained by dropping the x component from Eq. (87). If this vector were called \vec{S}_e'' , then the angle between it and the vector \hat{W}_e

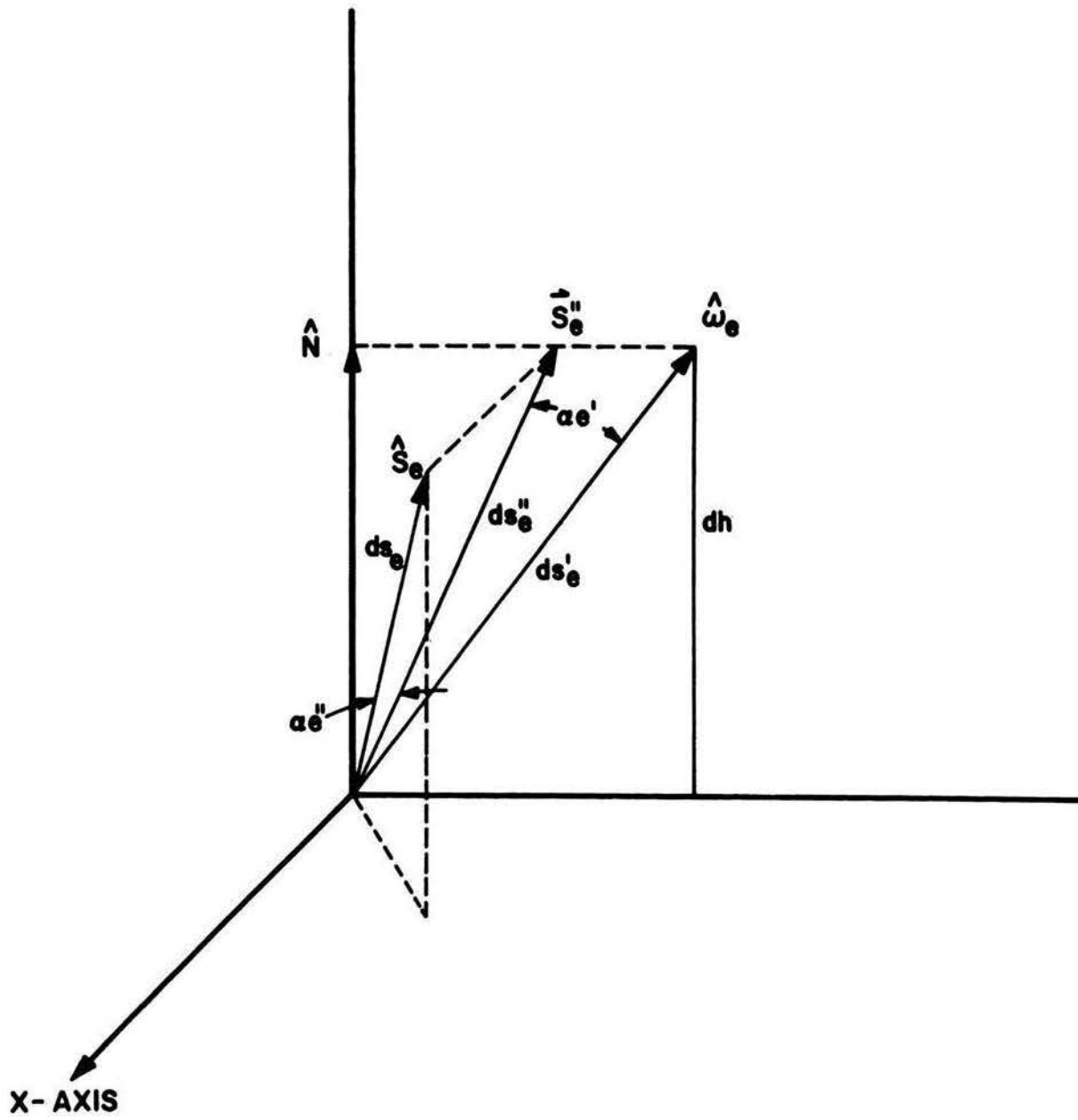


FIGURE 14 - RELATION BETWEEN dh AND dS_e

can be found from the relation

$$\sin \alpha'_e = \frac{\vec{S}_e'' \times \hat{W}_e \cdot \hat{i}}{|\vec{S}_e''|}$$

where the cross product has been used so that sign of the angle can be determined.

The result of the intermediate step is a differential length given by

$$ds_e'' = \frac{dh}{\cos(\chi_e + \alpha_e)} \quad (91)$$

This length is the projection of the ray path length on to the y-z plane, and its relation to the ray path length is

$$ds_e' = \frac{ds_e''}{\cos \alpha_e''} \quad (92)$$

where the angle α_e'' can be found from the relation

$$\cos \alpha_e'' = \frac{\vec{S}_e \cdot \vec{S}_e''}{|\vec{S}_e''|} \quad (93)$$

Combining Eqs. (90) and (92) gives

$$ds_e = \frac{dh}{\cos(\chi_e + \alpha_e) \cos \alpha_e''} \quad (94a)$$

This expression can be written as

$$ds_e = \frac{dh}{\{ [1 - \sin^2 \chi_e]^{1/2} \cos \alpha_e' - \sin \chi_e \sin \alpha_e' \} \cos \alpha_e''} \quad (94b)$$

The angle χ_e is the angle of incidence at the spherical stratifications, and, since it still changes according to Snell's law, it is

possible to use an expression similar to Eq. (68). In this case, the expression would be

$$\sin \chi_e = \left(\frac{R}{R+h} \right) \frac{\sin \chi_{ef}}{\mu_e} \quad (95)$$

At this point it should be possible to utilize the assumption of nearly coincident ray paths and approximate χ_{ef} with the angle χ_f . Equation (95) then becomes

$$\sin \chi_e = \left(\frac{R}{R+h} \right) \frac{\sin \chi_f}{\mu_e}$$

and combining this with Eq. (94) gives

$$dS_e = \frac{\mu_e dh}{\left\{ \left[\mu_e^2 - \left(\frac{R}{R+h} \right)^2 \sin^2 \chi_f \right]^{\frac{1}{2}} \cos \alpha_e' - \left(\frac{R}{R+h} \right) \sin \chi_f \sin \alpha_e' \right\} \cos \alpha_e''} \quad (96)$$

The same procedure applied to the ordinary path leads to

$$dS_o = \frac{\mu_o dh}{\left\{ \left[\mu_o^2 - \left(\frac{R}{R+h} \right)^2 \sin^2 \chi_f \right]^{\frac{1}{2}} \cos \alpha_o' - \left(\frac{R}{R+h} \right) \sin \chi_f \sin \alpha_o' \right\} \cos \alpha_o''} \quad (97)$$

where

$$\sin \alpha_o' = \frac{\vec{S}_o'' \times \hat{W}_o}{|\vec{S}_o''|} \cdot \hat{i}$$

$$\cos \alpha_o'' = \frac{\hat{S}_o \cdot \vec{S}_o''}{|\vec{S}_o''|}$$

V. THE FARADAY ROTATION AND DISPERSIVE
DOPPLER EQUATIONS

With the results of the last section it is possible to write integral equations for the Faraday rotation and dispersive Doppler effects which should be reasonably accurate. From Eqs. (34), (52), (96), and (97), the number of rotations in the plane of polarization of a signal after transmitting through a given ionosphere is

$$\Omega = \frac{f}{2c} \int_0^{h_s} \frac{\mu_o^2 \cos \alpha_o dh}{\left\{ \left[\mu_o^2 - \left(\frac{R}{R+h} \right)^2 \sin^2 \chi_f \right]^{\frac{1}{2}} \cos \alpha_o' - \left(\frac{R}{R+h} \right)^2 \sin \chi_f \sin \alpha_o' \right\} \cos \alpha_o''} - \frac{f}{2c} \int_0^{h_s} \frac{\mu_e^2 \cos \alpha_e dh}{\left\{ \left[\mu_e^2 - \left(\frac{R}{R+h} \right)^2 \sin^2 \chi_f \right]^{\frac{1}{2}} \cos \alpha_e' - \left(\frac{R}{R+h} \right)^2 \sin \chi_f \sin \alpha_e' \right\} \cos \alpha_e''} \quad (98)$$

From Eqs. (64) and (75), the number of dispersive Doppler cycles observed during a time interval Δt is given by

$$F \Delta t = \frac{f}{c} \int_{t_1}^{t_2} \frac{\mu_{mf}^2 dh}{\left[\mu_{mf}^2 - \left(\frac{R}{R+h} \right)^2 \sin^2 \chi_{mf} \right]^{\frac{1}{2}}} - \frac{f}{c} \int_{t_1}^{t_2} \frac{\mu_f^2 dh}{\left[\mu_f^2 - \left(\frac{R}{R+h} \right)^2 \sin^2 \chi_f \right]^{\frac{1}{2}}} - \frac{f}{c} \int_{t_2}^{t_1} \frac{\mu_{mf}^2 dh}{\left[\mu_{mf}^2 - \left(\frac{R}{R+h} \right)^2 \sin^2 \chi_{mf} \right]^{\frac{1}{2}}} + \frac{f}{c} \int_{t_2}^{t_1} \frac{\mu_f^2 dh}{\left[\mu_f^2 - \left(\frac{R}{R+h} \right)^2 \sin^2 \chi_f \right]^{\frac{1}{2}}} \quad (99)$$

It is convenient to group this equation into two terms. Thus,

let

$$C = \frac{f}{c} \int_0^{h_s} \frac{\mu_{mf}^2 dh}{\left[\mu_{mf}^2 - \left(\frac{R}{R+h} \right)^2 \sin^2 \chi_{mf} \right]^{\frac{1}{2}}} - \frac{f}{c} \int_0^{h_s} \frac{\mu_f^2 dh}{\left[\mu_f^2 - \left(\frac{R}{R+h} \right)^2 \sin^2 \chi_f \right]^{\frac{1}{2}}} \quad (100)$$

where C is interpreted as the number of cycles the upper and lower frequencies are out of phase at a single instant during propagation through a given ionosphere. The number of dispersive Doppler cycles observed during Δt then becomes

$$F \Delta t = C_1 - C_2$$

It is obvious that these equations are useless without a previous knowledge of the ionosphere. In the program of analysis which uses these equations to evaluate actual data for the electron content, this difficulty is solved by evaluating the equations with a model ionosphere. The model selected is the α -Chapman [10] and is given by

$$N = N_{max} \exp[\frac{1}{2}(1 - Q - e^{-Q})] \quad (101)$$

where

N = the electron density at height h

N_{max} = the maximum electron density

$Q = (h - h_m) / H$

h_m = the height of maximum ionization

H = the scale height [11]

The model has the convenient property that its integrated electron density is proportional to N_{max} , that is,

$$N_T = \int_0^{h_s} N dh = N_{max} \int_0^{h_s} \exp[\frac{1}{2}(1 - Q - e^{-Q})] dh \quad (102)$$

A second quantity which cannot be directly measured and must be evaluated from a model is the geomagnetic field. The model used is a sixth-order spherical harmonic expansion [12] . It can give rather accurate values for the direction and the magnitude of the geomagnetic field at any point within the ionosphere. Unfortunately, the Gaussian coefficients [13] used in these calculations are rather out of date, being epoch 1955, but it is anticipated this will be corrected in future work.

The integrals are evaluated according to an eight-step Simpson integration scheme. While this is not the most accurate method, the results should be quite reliable. All of the integrands in question are slowly varying functions with only one inflection point and are approximately parabolic in shape.

The question of the effect of using the α -Chapman model to represent the actual ionosphere arises. The subject has been studied in detail by several authors [14] (using equations different from those presented here), and it has been concluded that varying the height of maximum ionization has only a very small effect upon the value of the integrated electron density and the number of Faraday rotations. This implies that the Faraday rotation effect is relatively independent of the

shape of the ionosphere, and that it is only dependent upon the integrated electron density.

Another interesting property of Faraday rotation and dispersive Doppler is that both phenomena vary almost linearly with increasing electron content. That this is true for Faraday rotation can be seen from Eq. (53). A similar expression can be derived for the dispersive Doppler equations; however, to substantiate the assumption even further, Eq. (100) was plotted as a function of N_{max} . It will be recalled from Eq. (102) that N_T is directly proportional to N_{max} ; hence, Figure 15 can also be considered to show the behavior of the dispersive Doppler effect for a varying electron content.

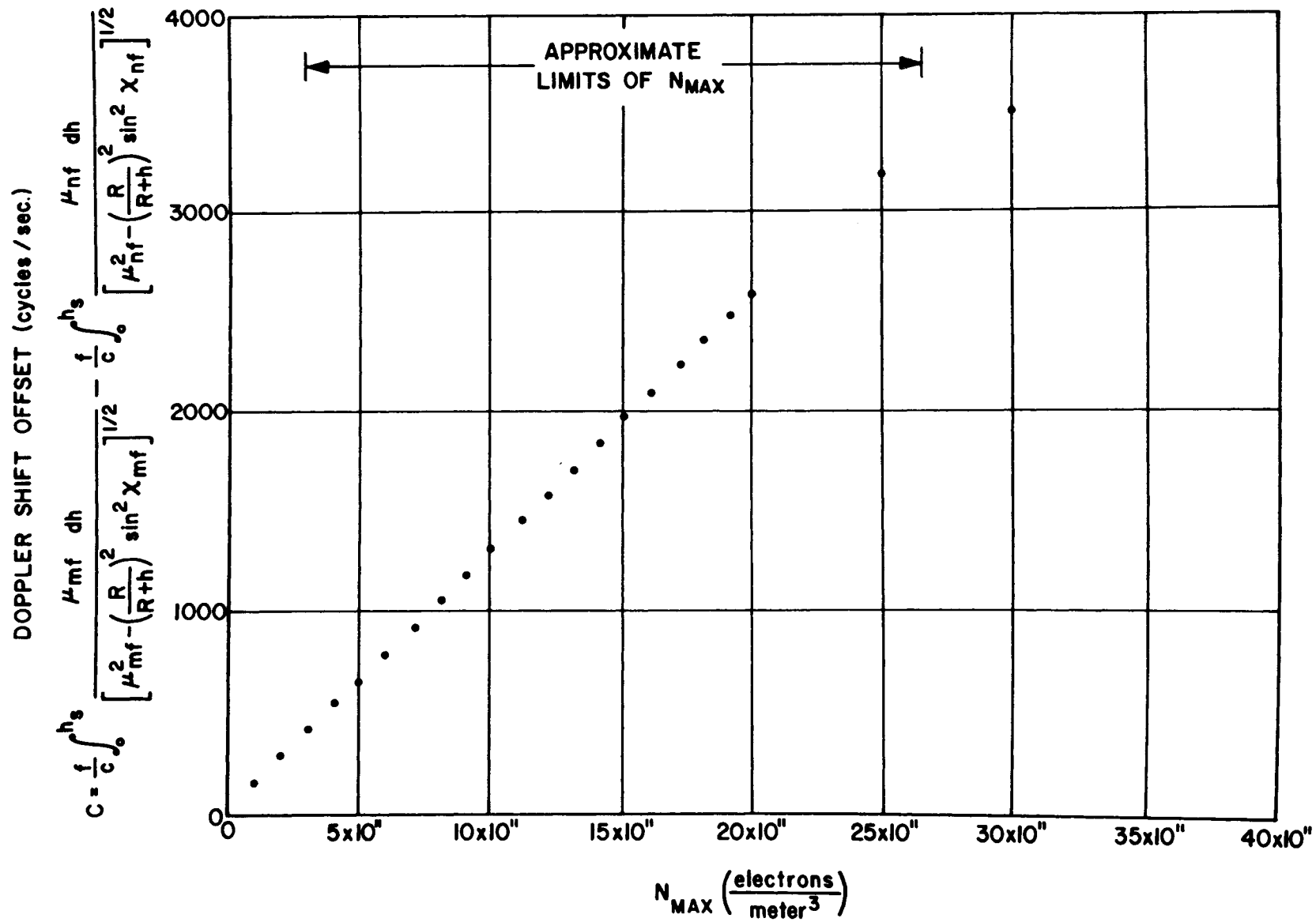


FIGURE 15 - DOPPLER SHIFT OFFSET VS. N_{MAX}

VI. METHOD OF ANALYSIS

The observed time rate of change of the Faraday rotation angle and Doppler shift offset is the result of two separate events. The first of these, the changing geometry as the satellite moves overhead, can be calculated with the equations and techniques of the previous section. The second event, a change in the electron content of the ionosphere (either with time or with position), is unknown and must be determined from the data. When neglected, rather modest gradients in the electron content can introduce errors in excess of fifty per cent into the analysis. However, since it was assumed in the derivations of the equations of the Faraday rotation and dispersive Doppler effects that no horizontal gradients were present in the ionosphere, the gradients which are detected will be attributed in the calculations to a time rate of change of the ionosphere. It is then necessary to utilize the equations in such a manner that the effects of possible horizontal gradients will be minimized.

The data which are read from the recorded charts are the number of dispersive Doppler cycles and the change in the Faraday rotation angle observed during the time interval between some t_1 and t_2 . If

the times t_1 and t_2 are selected so they coincide with adjacent signal level minimums in the AGC record (Figure 2 or Figure 3), then it is possible to write

$$\Omega_1 - \Omega_2 = \pm \frac{1}{2} \quad (103)$$

$$F\Delta t = c_1 - c_2 = \pm \eta \quad (104)$$

Using Eq. (101) for a model ionosphere and selecting some starting value for N_{max} , Eqs. (98) and (100) are used to calculate the quantities Ω'_1 and c'_1 at the geometry of time t_1 and Ω'_2 and c'_2 at the geometry of time t_2 .

The value of these quantities cannot be considered to be very close to the value of the corresponding quantities in Eqs. (103) and (104), however, because of the almost linear dependence of Ω and c upon N_T , it should be true that the ratio of Ω' and c' is close to the ratio of Ω and c . Thus, the quantities

$$G_1 \equiv \frac{\Omega_1}{c_1} \approx \frac{\Omega'_1}{c'_1} \quad (105)$$

$$G_2 \equiv \frac{\Omega_2}{c_2} \approx \frac{\Omega'_2}{c'_2} \quad (106)$$

are defined and calculated.

It is possible to solve Eqs. (105) and (106) and the equation

$$\frac{\Omega_1 - \Omega_2}{C_1 - C_2} = \pm \frac{1/2}{\eta} \quad (107)$$

for the term

$$\frac{\Omega_1}{\Omega_2} = \frac{G_1}{G_2} \left(\frac{G_2 \eta \pm 1/2}{G_1 \eta \pm 1/2} \right) \quad (108)$$

Barring the possibility of very large ionospheric gradients, it is possible to determine the signs from the relative values of Ω'_1 , Ω'_2 , C'_1 and C'_2 .

Once the ratio between Ω_1 and Ω_2 has been determined, it is tempting to solve Eqs. (108) and (103) for the number of Faraday rotations at times t_1 and t_2 . This operation produces reasonably accurate results when the ratio in Eq. (108) is sufficiently different from unity. However, when the number of Faraday rotations becomes fairly large (greater than thirty or forty) a slight inaccuracy in the value of Eq. (108) can cause several hundred per cent error in the results.

This ratio, however, contains information on the change in the electron content between times t_1 and t_2 . Recalling that the Faraday rotation effect is almost directly proportional to the electron content, it is possible, for the purpose of demonstration, to write

$$\Omega_1 = K_1 N_{T_1} \quad (109a)$$

$$\Omega_2 = K_2 N_{T_2} \quad (109b)$$

where the k_1 and k_2 are the geometrical constants of proportionality at times t_1 and t_2 , respectively.

It will be recalled that, in the original calculation of Ω_1' and Ω_2' , the same model ionosphere was used at both times t_1 and t_2 , thus

$$\Omega_1' = k_1 N_T \quad (110a)$$

$$\Omega_2' = k_2 N_T \quad (110b)$$

If the electron content of the model ionosphere is sufficiently close to the electron content of the real ionosphere, and if Eqs. (98) and (100) accurately describe the phenomena, then it can be argued that the constants in Eq. (109) are the same as the constants in Eqs. (110). If this is true, then,

$$\frac{\Omega_1}{\Omega_1'} = \frac{N_{T1}}{N_T}$$

$$\frac{\Omega_2}{\Omega_2'} = \frac{N_{T2}}{N_T}$$

and

$$E \equiv \frac{N_{T1}}{N_{T2}} = \frac{\Omega_1}{\Omega_1'} / \frac{\Omega_2}{\Omega_2'} \quad (111)$$

where E could be called the "ionosphere variation ratio."

Recalling the properties of the α -Chapman model ionosphere, it will be noted that Eq. (111) could be written

$$E = \frac{(N_{MAX})_1}{(N_{MAX})_2} \quad (112)$$

Equation (112) gives a convenient measure of the change in electron content between times t_1 and t_2 . It is now necessary to return to Eq. (98) and, with two model ionospheres which are constrained to meet the condition of Eq. (112), calculate new values for Ω'_1 and Ω'_2 . The value of $(N_{MAX})_1$ and $(N_{MAX})_2$ can then be iterated, still constrained by Eq. (112) until the difference between Ω'_1 and Ω'_2 is one-half rotation.

If the final values of $(N_{MAX})_1$ and $(N_{MAX})_2$ are appreciably different from the originally selected value of N_{MAX} , then it is advisable to repeat the entire process with a starting value of N_{MAX} based upon the results of this first set of calculations; otherwise, it is possible to take the integrated electron content of the two model ionospheres (N_{T1} and N_{T2}) to be the electron content of the ionosphere at times t_1 and t_2 .

A fundamental deficiency in the method becomes evident in the last step of the calculations. Since the integration has been over the variable h , rather than along the ray path, it is difficult to interpret the results. However, had the integration been performed along the ray path, the answer would have had very little value to the geophysicist. To correct for this in the best possible way, the value of N_{T1} and N_{T2} is

related to a location called the "subionosphere point." This point is related to the height of maximum ionization in the manner shown in Figure 16. It is around the point of maximum ionization that most of the contribution to the various integrands occurs, although it might be argued that the subionosphere point should be referred to the somewhat higher centroid of the α -Chapman model.

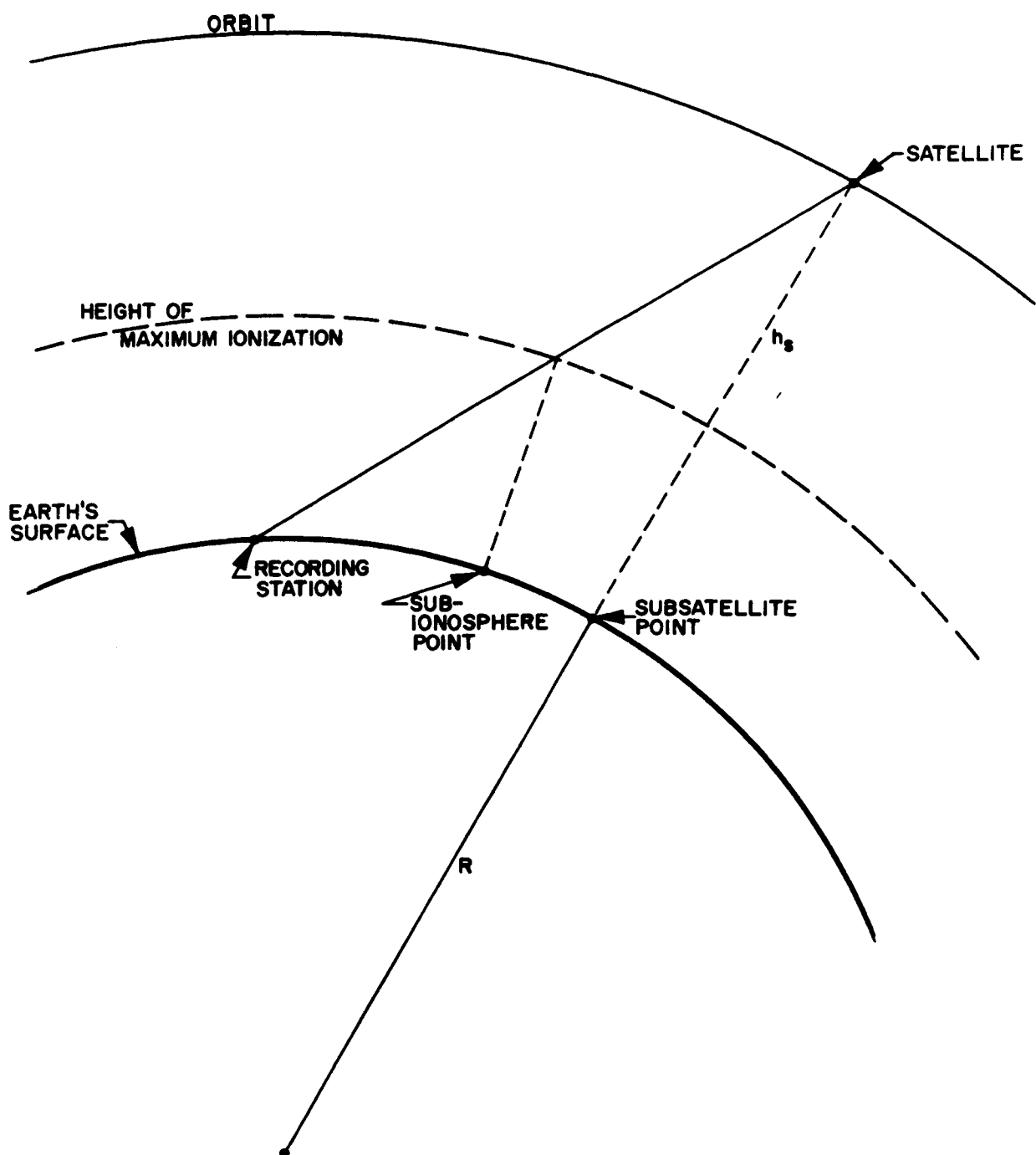


FIGURE 16 - SUBIONOSPHERE POINT

VII. RESULTS OF ANALYSIS

The data selected for the initial analysis were received from the Explorer 22 satellite on September 4, 1965, during the satellite's four thousand five hundred twenty-first orbit. During the orbit, the satellite was observed from the Green Mountain Station from approximately 10:15:30 CST to 10:31:30 CST. The pass over Green Mountain was from south to north with close approach to the station occurring at approximately 10:23 CST. Continuous reception of all four of the satellite's transmissions was maintained during the entire pass, but usable data were received only between 10:17 CST and 10:26 CST.

The pass was selected primarily because it occurred near mid-day when refraction effects are most serious, but it also had the advantage that the satellite was almost directly overhead during close approach. It was anticipated that a pass with a very high maximum elevation would be required to determine if there were errors in the analysis at low elevations.

It was possible to discern a change of twenty-four complete rotations (forty-eight data points) in the plane of polarization of the 40 MHz transmissions during the pass and one hundred twenty-four complete rotations in the plane of polarization of the 20 MHz transmissions .

Since experience has shown that analysis of both the 20 MHz and 40 MHz data lead to almost identical results, only the 40 MHz data were analyzed. The data and the orbital parameters of the satellite are listed in Table 1. The results of the analysis are listed in Table 2 and graphically represented in Figure 17.

As can be seen, the results of the analysis were discouraging.

Three separate types of errors are apparent in these results:

1. The agreement between adjacent points is not too good.
2. The results go toward infinity near the center of the data
3. The results at the end of the data disagree with those at the first by almost an order of magnitude.

The first of these errors can be traced to the computer program itself. At present, the program is rather clumsy and a considerable amount of error can build up in the various iterations. For example, it was possible for the calculated difference in the angle of arrival of the satellite's transmissions between two data points to be in error by as much as a quarter of a degree.

The second error is somewhat more serious, particularly since it occurs in the region of the sky where the angle between the ray path and the geomagnetic field goes to zero. It will be recalled that a major

TABLE 1

Recorded Data and the Position of the Satellite
Relative to the Green Mountain Station

OBSERVED DATA				SATELLITE POSITION AT t			
t				ELEV.	AZIMUTH	RANGE	HEIGHT
(Hr:Min:Sec)		(cycles)	(deg)	(deg)	(deg)	(km)	(km)
(GMT)							
1	16 17 26.52		9.34	186.99	2607.1	888.3	
2	32.20	9.30	9.80	186.98	2570.7	888.1	
3	38.01	9.52	10.28	186.96	2533.6	888.0	
4	43.68	9.50	10.76	186.95	2497.5	888.9	
5	49.81	9.33	11.28	186.93	2458.4	887.7	
6	56.52	10.60	11.88	186.92	2415.8	887.6	
7	18 3.56	10.10	12.51	186.90	2371.1	887.4	
8	10.68	9.95	13.17	186.87	2327.1	887.3	
9	17.76	10.15	13.84	186.85	2281.4	887.1	
10	25.80	10.75	14.63	186.82	2230.9	887.0	
11	34.36	11.00	15.50	186.79	2177.3	886.9	
12	42.70	11.40	16.37	186.78	2125.2	886.7	
13	50.58	10.85	17.23	186.72	2076.3	886.6	
14	58.51	10.50	18.12	186.69	2027.3	886.5	
15	19 6.38	10.50	19.04	186.65	1978.9	886.4	
16	14.33	11.00	20.00	186.60	1930.3	886.3	
17	22.28	10.75	21.00	186.56	1882.0	886.2	
18	30.72	11.00	22.10	186.50	1831.0	886.2	
19	39.46	10.80	23.30	186.44	1778.7	886.1	
20	48.22	10.75	24.56	186.37	1726.8	886.0	
21	56.50	10.51	25.80	186.30	1678.2	886.0	
22	20 4.97	10.51	27.14	186.23	1629.0	886.0	
23	13.19	10.40	28.50	186.14	1581.9	885.9	
24	21.24	10.00	29.90	186.05	1536.3	885.9	
25	29.21	10.00	31.35	185.95	1491.8	885.9	
26	37.41	10.15	32.92	185.84	1446.8	885.9	
27	45.70	10.00	34.60	185.71	1402.1	885.9	
28	53.65	9.45	36.30	185.57	1360.1	885.9	
29	21 2.98	9.80	38.41	185.39	1312.0	886.0	
30	14.70	10.80	41.25	185.12	1253.7	886.0	
31	25.94	9.65	44.20	184.80	1200.2	886.1	
32	37.84	9.40	47.59	184.39	1146.6	886.2	
33	51.97	9.55	51.98	183.75	1087.5	886.3	
34	22 4.96	8.40	56.39	182.96	1038.4	886.5	
35	18.14	7.50	61.25	181.82	994.4	886.6	
36	31.20	6.40	66.42	180.11	957.3	886.8	
37	44.45	5.50	71.98	177.22	927.2	887.0	
38	57.46	5.00	77.65	171.61	905.8	887.2	
39	23 10.62	2.80	83.24	156.14	892.9	887.5	
40	24.12	1.25	86.19	90.07	889.2	887.8	
41	37.64	0.00	81.92	37.08	895.2	888.1	
42	52.00	2.00	75.71	24.13	912.2	888.5	
43	24 8.06	5.40	68.81	18.91	943.4	888.9	
44	24.37	7.50	62.23	16.36	986.8	889.3	
45	40.86	9.80	56.12	14.86	1041.4	889.8	
46	57.34	9.40	50.62	13.90	1105.0	890.4	
47	25 13.63	10.00	45.74	13.24	1175.3	890.9	
48	29.60	10.40	41.46	12.76	1250.3	891.5	
49	46.23	12.35	37.46	12.39	1333.5	892.1	
50	26 4.28	14.86	33.61	11.90	1428.7	892.8	

TABLE 2
RESULTS OF ANALYSIS

	OBSERVED		CALCULATED	CALCULATED	
	(Hr; Min; Sec) (GMT)		$\frac{N_T}{m^2} \times 10^{-16}$	IONOSPHERE VARIATION RATIO	
1	16	17	26.52	7.98	.967
2			32.20	7.54	.964
3			38.01	9.47	.963
4			43.68	6.01	.959
5			49.81	7.74	.953
6			56.52	8.15	.948
7		18	3.56	7.95	.944
8			10.68	7.87	.943
9			17.76	8.99	.934
10			25.80	8.46	.924
11			34.36	9.16	.923
12			42.70	9.33	.923
13			50.58	9.14	.918
14			58.51	9.97	.915
15		19	6.38	9.51	.911
16			14.33	9.94	.906
17			22.28	9.54	.895
18			30.72	10.01	.885
19			39.46	10.63	.877
20			48.22	12.84	.875
21			56.50	13.47	.863
22		20	4.97	15.26	.856
23			13.19	18.31	.845
24			21.24	24.93	.832
25			29.21	41.59	.810
26			37.41	140.11	.784
27			45.70	136.20	.742
28			53.65	49.05	.667
29		21	2.98	112.32	.484
30			14.70	3.59	.183
31			25.94	6.83	-1.695
32			37.84	41.27	1.374
33			51.97	87.98	1.199
34		22	4.96	39.43	1.127
35			18.14	28.05	1.089
36			31.20	21.76	1.052
37			44.45	16.79	1.012
38			57.46	5.55	.995
39		23	10.62	6.48	.998
40			24.12	5.28	.992
41			37.64	8.06	1.003
42			52.00	5.24	1.030
43		24	8.06	4.86	1.032
44			24.37	4.72	1.031
45			40.86	3.81	1.000
46			57.34	2.74	.978
47		25	13.63	2.71	.954
48			29.60	2.79	.955
49			46.23	1.18	.969
50		26	4.28		

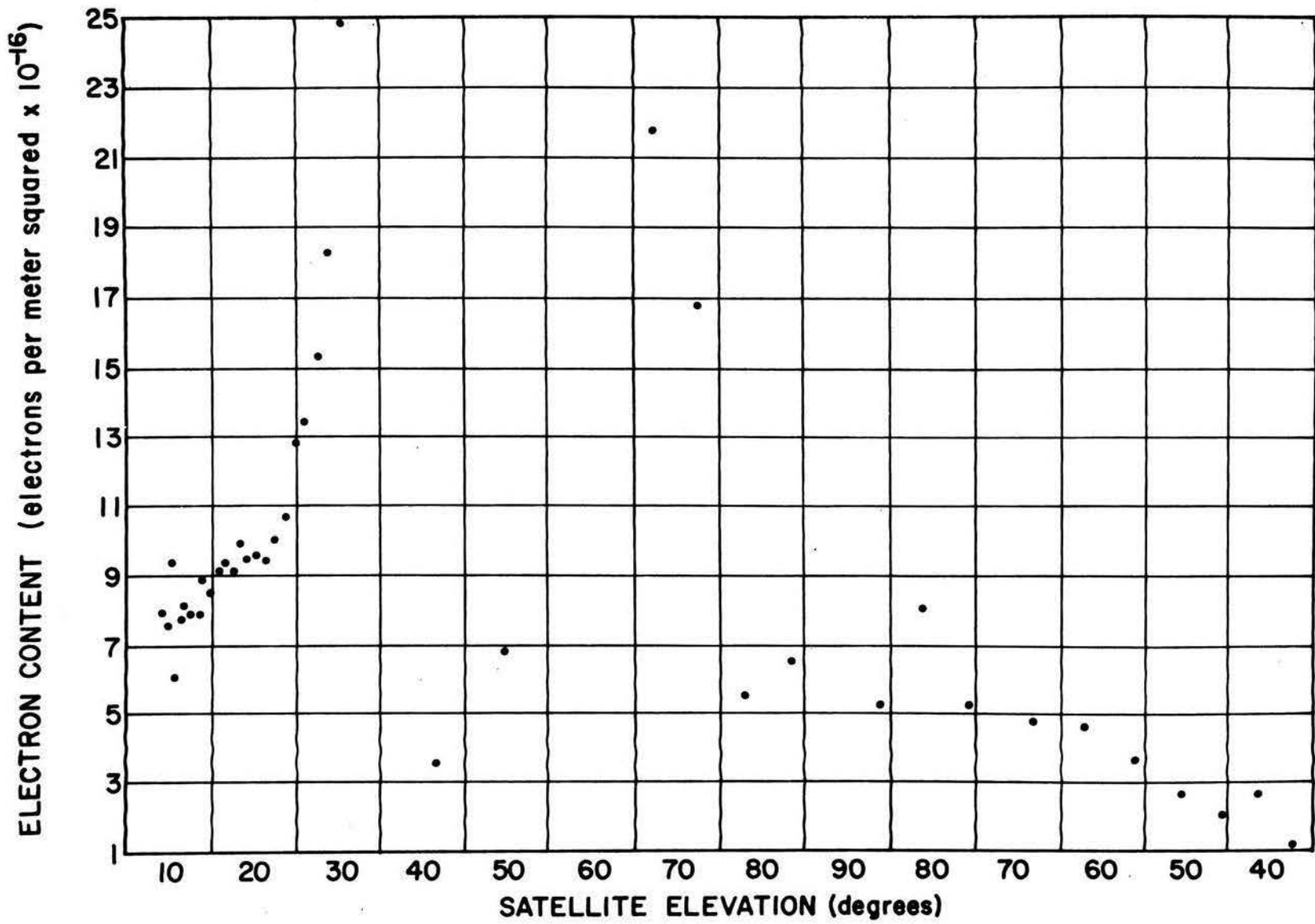


FIGURE 17 - ELECTRON CONTENT VS. SATELLITE ELEVATION

approximation employed in the derivation of the Faraday rotation equations is most accurate in this region of the sky and the results would be expected to be most accurate at this point.

The cause of the difficulty becomes evident if the ionosphere variation ratio is examined. The value the computer calculated for this term at each point is shown in Figure 18. It will be recalled from Eqs. (108) and (111) that the expression for this quantity is

$$E = \frac{G_1}{G_2} \left(\frac{G_2 \eta \pm 1/2}{G_1 \eta \pm 1/2} \right) / \left(\frac{\Omega'_1}{\Omega'_2} \right)$$

where

$$G_1 = \frac{\Omega'_1}{C'_1}$$

$$G_2 = \frac{\Omega'_2}{C'_2}$$

Combining these terms gives

$$E = \frac{\Omega'_2 \eta \pm \frac{1}{2} C'_2}{\Omega'_1 \eta \pm \frac{1}{2} C'_1} \quad (113)$$

Assuming, for simplicity, that t_1 and t_2 can be determined exactly, but that there is an error of $\Delta\eta$ in determining the number of dispersive Doppler cycles, then the error in E is given by

$$\Delta E = \frac{\Omega'_1 C'_2 \pm \Omega'_2 C'_1}{(\Omega'_1 \eta \pm \frac{1}{2} C'_1)^2} \frac{\Delta\eta}{2} \quad (114)$$

At the point where the discontinuity in E occurs both Ω and C are decreasing quantities. This requires the negative sign to be used. Thus,

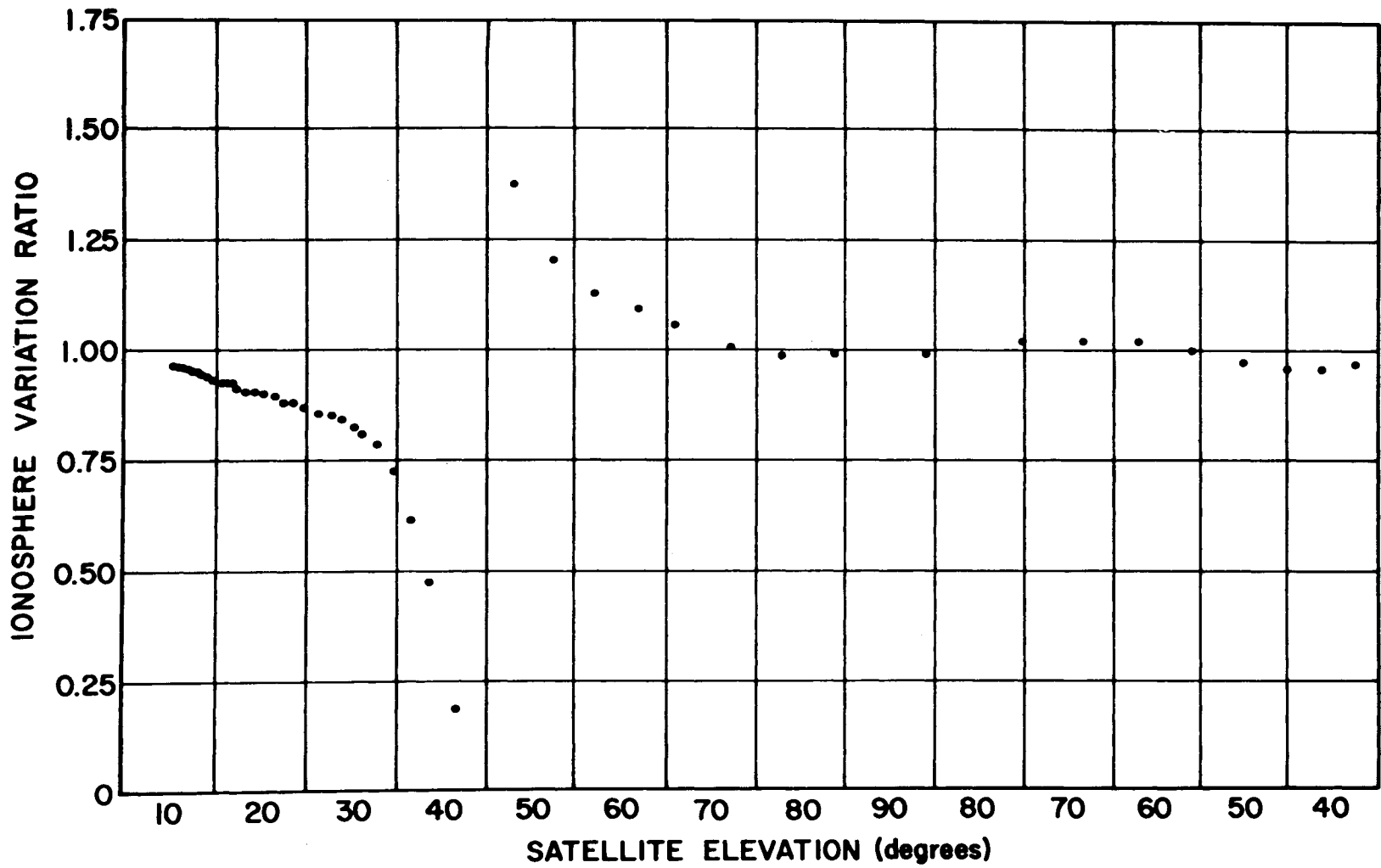


FIGURE 18 - IONOSPHERE VARIATION RATIO VS. SATELLITE ELEVATION

$$\Delta E = \frac{\Omega_1' c_2' - \Omega_2' c_1'}{(\Omega_1' \eta - \frac{1}{2} c_2')^2} \frac{\Delta \eta}{2}$$

where

$$\frac{1}{2} = \Omega_1 - \Omega_2$$

$$\eta = c_1 - c_2$$

Combining these expressions results in

$$\Delta E = \frac{(c_2' \Omega_1' - c_1' \Omega_2')}{[\Omega_1' (c_1 - c_2) - c_1' (\Omega_1 - \Omega_2)]^2} \frac{\Delta \eta}{2} \quad (115)$$

Since the angle between the ray path and the geomagnetic field is small and the satellite is at a fairly high elevation at this point, the approximation of straight-line propagation should be reasonably accurate. If this be true, then it can be shown, by means of the same approximations which led to Eq. (53), that

$$G = \frac{R}{c} \sim \cos \theta$$

This implies that

$$\Omega_1 = \kappa c_1 \cos \theta \quad (116a)$$

$$\Omega_1' = \kappa c_1' \cos \theta \quad (116b)$$

$$\Omega_2 = \kappa c_2 \cos \theta \quad (116c)$$

$$\Omega_2' = \kappa c_2' \cos \theta \quad (116d)$$

where the κ is now the constant of proportionality between the Faraday rotations and dispersive Doppler cycles and the primes are to indicate that the quantities are calculated from a model.

Combining Eqs. (115) and (116), and grouping the term, gives

$$\Delta E = \frac{C_1' C_2' (\cos \theta_1' - \cos \theta_2')}{k [C_1 C_1' (\cos \theta_1' - \cos \theta_1) + C_1' C_2 (\cos \theta_2 - \cos \theta_1')]^2} \frac{\Delta \eta}{2} \quad (117)$$

Substituting the expressions

$$\theta_1 - \theta_1' = \pm \Delta \theta$$

$$\theta_2 - \theta_2' = \pm \Delta \theta$$

into Eq. (117), and applying the small angle approximations, gives

$$\Delta E = \frac{C_1' C_2' (\cos \theta_1' - \cos \theta_2')}{k [C_1' C_2 (\cos \theta_2 - \cos \theta_1') \pm C_1' \Delta \theta (C_1 \sin \theta_1' - C_2 \sin \theta_2')]^2} \frac{\Delta \eta}{2} \quad (118)$$

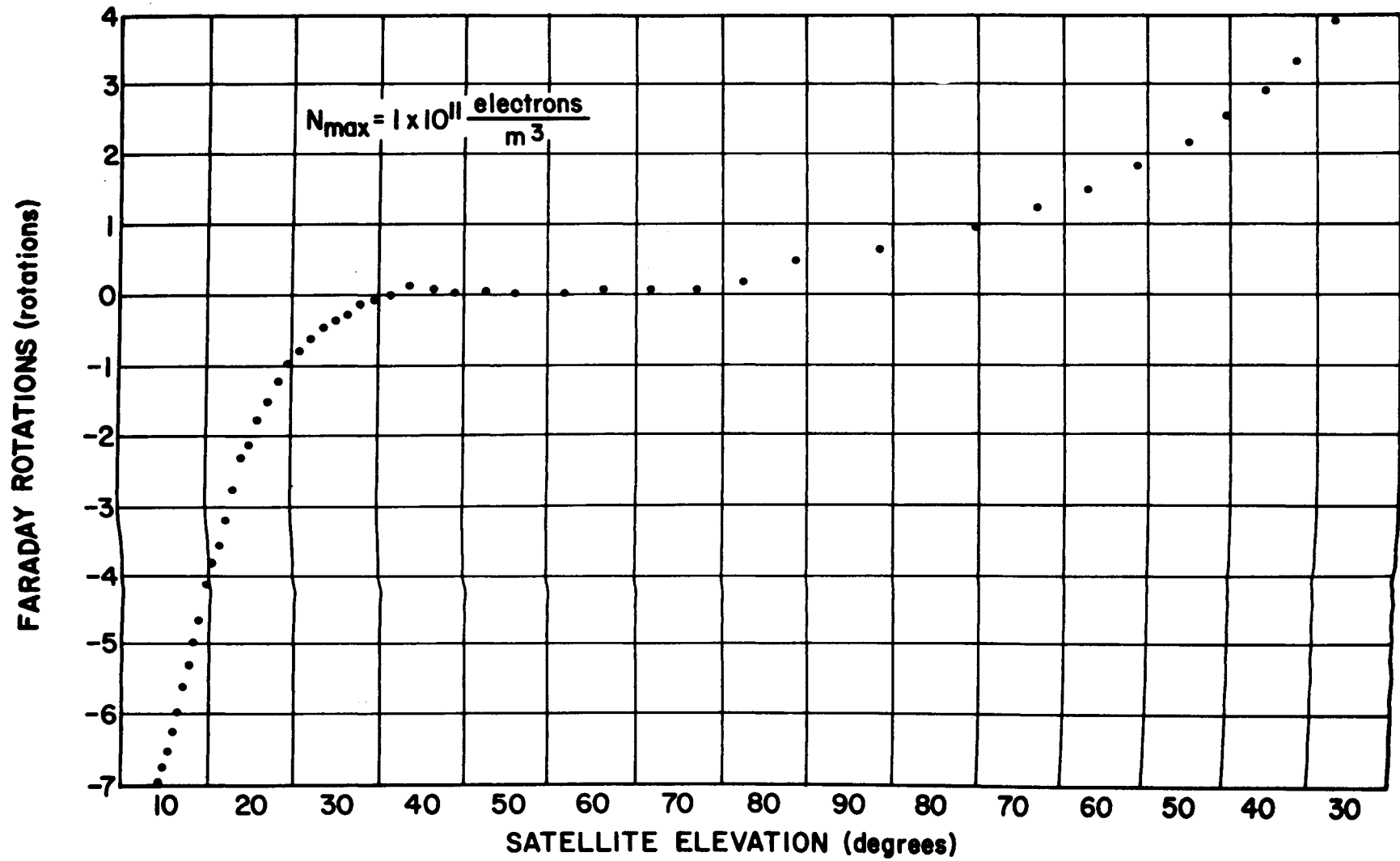
The cause of the discontinuity in the ionosphere variations ratio now becomes apparent. In the region where the discontinuity occurs, the angle θ is going through a minimum. Only when $\Delta \theta$ is zero can both the numerator and denominator of Eq. (118) reach zero simultaneously. This, of course, is possible only if the model of the geomagnetic field is exact.

It is apparent from Figure 18 that the model of the geomagnetic field used in these calculations was too inaccurate to lead to reliable results. It is doubtful that it will be possible to obtain a model accurate enough to entirely eliminate this source of error to the point where it can be tolerated. Otherwise, it will be necessary to develop a method of analysis which is not so critically dependent upon the accuracy of the geomagnetic field model.

Since the third error appears in the results at the point where the angle between the ray path and the geomagnetic field is becoming fairly large, it seems reasonable to attribute it to the Q-L approximation. Various authors disagree on the use of the approximation, but the most thorough study [14] indicates that under the conditions existing at the time these data were recorded, the approximation would become invalid below an elevation of about fifty degrees to the north. If so, the results of the last four or five calculations would have to be considered inaccurate.

It is of interest to examine the calculated behavior of Ω with a constant ionosphere as the satellite moves across the sky. The results of such a calculation are shown in Figure 19. The calculations were made with the regular analysis program using the recorded data, but with N_{MAX} fixed to the same value at each point.

The value of Ω began negative (indicating the extraordinary phase path was longer than the ordinary phase path), increased through zero to a maximum, decreased for several points, and then continued increasing. At the two points where $d\Omega/dt$ changed sign, the chart record was examined but there was nothing unusual about the data at that point. However, in both cases, the preceding data point did exhibit a peculiarity. In the two cases, the variation in the recorded



signal level of the 40 MHz beacon did not have the smooth, sinusoidal appearance typical of the data in Figures 2 and 3. In both cases, it was evident that $d\Omega/dt$ was going through some type of rapid change. These were the only points on the chart where the recording of the 40 MHz signal level exhibited this phenomenon.

Although it is not possible to definitely conclude that the direction of rotation of the plane of polarization with respect to the fixed dipole antenna actually reversed at these two points, it seems rather likely. If the model of the geomagnetic field used in the calculations was in error (a fact which has been established) it would be possible to account for the displacement between the calculations and the observed data.

VIII. CONCLUSIONS

The several errors which occurred in the numerical calculations make it difficult to determine the validity of the method. However, since it was possible to determine the source of these errors, it seems likely that it will be possible to obtain accurate results once corrections are made. The value determined for the electron content in the early portion of the data is quite reasonable and it would be plausible for a gradient to exist which would account for the difference in electron content between the early part of the pass and the time of close approach.

The most interesting results of the analysis was the behavior of Ω as the satellite moved across the sky. If a similar calculation is made using Eq. (53) the results are drastically different. In this case, Ω is found to be at a maximum in the southern part of the sky and decreasing monotonically to zero toward the northern part of the sky where the ray path and the geomagnetic field are perpendicular. The same general behavior is exhibited if the phase difference is evaluated by integrating the difference in the two refractive indices along the straight line between the receiver and the satellite.

However, when the corrections for path bending and splitting are included in the integral equations, then the relative geometrical

lengths of the two-phase paths become a dominating factor. In the northern part of the sky the refractive and anisotropic terms combine to make the geometrical length of the extraordinary ray path shorter than the geometrical length of the ordinary ray path, while the opposite is true in the southern part of the sky.

It is felt that the apparent ability of the equation which includes these effects to accurately predict changes in the direction of rotation of the plane of polarization with respect to the receiving antenna is a definite indication of its validity.

IX. BIBLIOGRAPHY

1. Garriott, O.K., The determination of ionospheric electron content and distribution from satellite observations, J. Geophys. Res., 65 1139-1150, 1960.
2. Lawrence, R. S. and D. J. Posakony, A digital ray-tracing program for ionospheric research, Proc. Intern. Space Sci. Sympos., 2nd, 258-276, 1961.
3. Budden, K. G., Radio Waves in the Ionosphere (Cambridge University Press, Cambridge, 1961).
4. Ratcliffe, J. A., The Magneto-Ionic Theory and Its Applications to the Ionosphere (Cambridge University Press, Cambridge, 1961).
5. Jackson, J. D., Classical Electrodynamics (John Wiley and Sons, New York, 1962).
6. Davies, K., Ionospheric Radio Propagation (U.S. Government Printing Office, Washington, 1965).
7. Mechtly, E. A., Lecture presented at Marshall Space Flight Center, Huntsville, Alabama, 1963.
8. Kelso, J. M., Radio Ray Propagation in the Ionosphere (Mcgraw-Hill, New York, 1964).
9. Kelso, J. M., Doppler shifts and Faraday rotation of radio signals in a time-varying, inhomogeneous ionosphere, J. Geophys. Res., 66, 1107-1115, 1961.

10. Ratcliffe, J. A., Physics of the Upper Atmosphere (Academic Press, New York, 1960).
11. Seddon, J. C., A model of the quiet ionosphere, J. Geophys. Res., 68, 1339-1345, 1963.
12. Jones, H. S. and P. J. Melotte, The harmonic analysis of the earth's magnetic field, M. N. Geophys. Suppl., 6, 409-430, 1953.
13. Finch, H. F. and B. R. Leaton, The earth's main magnetic field — epoch 1955, M. N. Geophys. Suppl., 7, 314-317, 1957.
14. Potts, B. C., Mean ionospheric scale heights deduced from Faraday rotation measurements, J. Geophys. Res., 70, 2651-2663, 1965.

X. VITA

The investigator of this research, Charles Roland Baugher, II, was born in Joplin, Missouri, on September 21, 1941. He received his elementary and high school education in the public schools of Neosho, Missouri. In September of 1959, he entered the University of Missouri at Rolla, Missouri, and in May of 1963, he received his Bachelor of Science Degree in Engineering Physics.

Upon graduation Mr. Baugher became a graduate cooperative student with the National Aeronautics and Space Administration's George C. Marshall Space Flight Center at Huntsville, Alabama where the research which preceded his Master of Science thesis was accomplished.